National Library of Canada
Acquisitions and Bibliographic Services Branch
395 Wellington Street
Ottawa, Ontario
K1A 0N4

Bibliothèque nationale du Canada
Direction des acquisitions et des services bibliographiques
395, rue Wellington
Ottawa (Ontario)
K1A 0N4

Your file Votre référence

Our file Notre référence

NOTICE

The quality of this microform is heavily dependent upon the quality of the original thesis submitted for microfilming. Every effort has been made to ensure the highest quality of reproduction possible.

If pages are missing, contact the university which granted the degree.

Some pages may have indistinct print especially if the original pages were typed with a poor typewriter ribbon or if the university sent us an inferior photocopy.

Reproduction in full or in part of this microform is governed by the Canadian Copyright Act, R.S.C. 1970, c. C-30, and subsequent amendments.

AVIS

La qualité de cette microforme dépend grandement de la qualité de la thèse soumise au microfilmage. Nous avons tout fait pour assurer une qualité supérieure de reproduction.

S'il manque des pages, veuillez communiquer avec l'université qui a conféré le grade.

La qualité d'impression de certaines pages peut laisser à désirer, surtout si les pages originales ont été dactylographiées à l'aide d'un ruban usé ou si l'université nous a fait parvenir une photocopie de qualité inférieure.

La reproduction, même partielle, de cette microforme est soumise à la Loi canadienne sur le droit d'auteur, SRC 1970, c. C-30, et ses amendements subséquents.

Canada

UNIVERSITY OF ALBERTA

FLEXIBLE COMPOSITE TUBULAR STRUCTURE

BY

SHE, SIU NANG

©

A thesis submitted to the Faculty of Graduate Studies and Research in partial fulfilment of the requirements for the degree of Master of Science.

DEPARTMENT OF MECHANICAL ENGINEERING

Edmonton, Alberta

Spring, 1993

National Library
of Canada

Acquisitions and
Bibliographic Services Branch

395 Wellington Street
Ottawa, Ontario
K1A 0N4

Bibliothèque nationale
du Canada

Direction des acquisitions et
des services bibliographiques

395, rue Wellington
Ottawa (Ontario)
K1A 0N4

Your file Votre référence

Our file Notre référence

The author has granted an irrevocable non-exclusive licence allowing the National Library of Canada to reproduce, loan, distribute or sell copies of his/her thesis by any means and in any form or format, making this thesis available to interested persons.

L'auteur a accordé une licence irrévocable et non exclusive permettant à la Bibliothèque nationale du Canada de reproduire, prêter, distribuer ou vendre des copies de sa thèse de quelque manière et sous quelque forme que ce soit pour mettre des exemplaires de cette thèse à la disposition des personnes intéressées.

The author retains ownership of the copyright in his/her thesis. Neither the thesis nor substantial extracts from it may be printed or otherwise reproduced without his/her permission.

L'auteur conserve la propriété du droit d'auteur qui protège sa thèse. Ni la thèse ni des extraits substantiels de celle-ci ne doivent être imprimés ou autrement reproduits sans son autorisation.

ISBN 0-315-95111-7

Canada

UNIVERSITY OF ALBERTA

RELEASE FORM

NAME OF AUTHOR: Siu Nang She

TITLE OF THESIS: Flexible Composite Tubular Structure

DEGREE: Master of Science

YEAR THIS DEGREE GRANTED: Spring 1993

Permission is hereby granted to the University of Alberta Library to reproduce single copies of this thesis and to lend or sell such copies for private, scholarly or scientific research purposes only.

The author reserves all other publication and rights in association with the copyright in the thesis, and expect as hereinbefore provided neither the thesis nor any substantial portion thereof may be printed or otherwise reproduced in any material from whatever without the author's prior written permission.

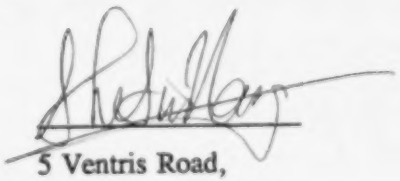

5 Ventris Road,
Flat C2, 22/F
Happy Valley
Hong Kong

Date: 11 Mar. 93'

UNIVERSITY OF ALBERTA

FACULTY OF GRADUATE STUDIES AND RESEARCH

The undersigned certify that they have read, and recommend to the Faculty of Graduate Studies and Research for acceptance, a thesis entitled **Flexible Composite Tubular Structure** submitted by **Siu Nang She** in partial fulfilment of the requirements for the degree of Master of Science.

Dr. D.R. Budney (Supervisor)

Dr. A.W. Lipsett

Dr. T.M. Hrudey

Date: March 11, 1993

Abstract

The objective of this thesis was to investigate the behaviour of a flexible composite structure, including the contribution of the liner as a structural layer, under different loading conditions. In a previous study, the engineering report of Composite Technologies Inc., the liner stiffness was neglected. This thesis includes analysis of the structural response of the pipe to temperature change. Design of pipe test specimens and pressure testing of these specimens were also included in the scope of this thesis. Prototypes were designed and manufactured, using the basic stress analysis of the engineering report. Two prototypes, one of which was designed for zero longitudinal strain and zero rotation when pressurized with unrestrained ends, were constructed and tested, the second prototype was designed to allow axial growth.

The author of this thesis also contributed to the development of an end connection for the flexible pipe. This enables the pipe to be connected to a standard flange used in the steel pipe industry. The end connection design and related assembly procedures are described in this thesis.

The hydrostatic tests followed procedures recommended by ASTM standards. Some special testing facilities were developed for this test. Discussion of these facilities, testing procedures, data, results and failure analysis are included.

The first prototype burst at a pressure of 3,000 psi in an unrestrained end test. Failure analysis of the prototype is included in the thesis. Valuable information was obtained from the results and observations of the hydrostatic pressure test. This information was used to modify the prototype design and the end connection. The modified prototype was successfully tested to 5,000 psi internal pressure. The design modifications on the pipe and the end connection are included in this thesis. Recommendations for future pipe development and further study are also outlined.

Acknowledgements

I would like to thank my thesis supervisor, Dr. D.R. Budney, for his advice and guidance. The financial support provided by my thesis supervisor is also gratefully acknowledged.

The technical assistance of Brain Cielin, Bernie Faulkner, Ian Buttar, Terry Nord, John Foy and, Tuula Hilvo of the Department of Mechanical Engineering and of Alan Muir, Max Schubert, Don Fuhr, Tony van Straten, and Albert Yuen of Technical Services was very much appreciated.

Finally, I would like to thank the Mechanical Engineering Department of the University of Alberta and Mr. Don Wolfe of Composite Technologies Inc. for providing the financial assistance. This project is supported by Composite Technologies Inc.

Table of Contents

List of Tables . . . . .

List of Figures . . . . .

List of Symbols . . . . .

Chapter 1 Introduction 1
Chapter 2 Theory 3
2.1 Simple model 3
2.2 Complex model 6
2.3 Stress analysis including behaviour of liner 15
2.4 Prototype design 25
2.5 Calculations for pipe "C" (including the liner behaviour) at 5,000 psi 28
Chapter 3 Thermal Effect 42
3.1 Simple model 42
3.2 Complex model 46
3.3 Thermal stress of an actual pipe 51
Chapter 4 End Connection 56
4.1 End connection design 56
4.2 End connection mechanisms 61
Chapter 5 Testing Facilities and Testing Procedure 63
5.1 Testing facilities 63
5.2 Testing procedure 66
Chapter 6 Results and Discussion 74
6.1 Data and observations 74
6.2 Calculation results and discussion 77
Chapter 7 Pipe Modification 82
7.1 Pipe design and end connection modifications 82
7.2 Testing procedure and test results 85
Chapter 8 Conclusion and Recommendations 88
8.1 Conclusion 88
8.2 Recommendations 89
Bibliography 91

List of Tables

Table 2.1 Designed parameters of pipe "C" 25

Table 2.2 Manufactured parameters of pipe "C" 26

Table 2.3 Calculation for pipe "C" at 5,000 psi 27

Table 2.4 Calculations for pipe "C" (including behaviour of the liner) at 5,000 psi 29

Table 3.1 Calculations for pipe "C" when temperature increases in the liner and the structural layers are common at 130°F 55

Table 3.2 Calculations for pipe "C" when temperature increases in the liner and the structural layers are common at 130°F after the liner undergoes load relaxation 55

Table 6.1 Measurements taken in testing of pipe "C" 74

Table 6.2 Calculations for pipe "C" under restrained capped ends condition at 3,000 psi internal pressure 77

Table 7.1 Designed parameters of pipe "D3" 83

Table 7.2 Measurements taken in testing of pipe "D3" 86

List of Figures

Figure 2.1 Simple model. The liner, which serves as a non-structural barrier to internal pressure is not shown. α is shown as the fraction of composite in a layer for one strip width. t is the radial thickness of a layer. 30

Figure 2.2A Transverse plane of a simple model, axial loading of the structural layers (Only the ends of some helical strips are shown.). 31

Figure 2.2B Sectioned diametral plane of half structural layers in a simple model, radial loading (Only the ends of some helical strips are shown.) . 31

Figure 2.3 Complex model with structural strips and liner only, elastomer strips are not shown.. 32

Figure 2.4 Basic hoop layer construction, composite strips are separated by elastomer strips. 33

Figure 2.5 Basic helix layer construction, composite strips are separated by elastomer strips 33

Figure 2.6A Sectioned diametral plane of half hoop layers in a complex model, radial loading of hoop layers (Only the ends of some strips are shown). 34

Figure 2.6B Sectioned diametral plane of half helix layers in a complex model, radial loading of helix layers (Only part of the strips is shown.) Internal pressure p_c is applied by the hoop layers. 34

Figure 2.6C Transverse plane of a complex model, axial loading of the structural layers. 35

Figure 2.7 Torque generated by a single hoop layer of a complex model. T_o is the torque generated by the hoop layer. 35

Figure 2.8A Geometry of one helical pitch. 36

Figure 2.8B Development view of one pitch of a strip. 36

Figure 2.9 Schematic of longitudinal pipe deformation. 37

Figure 2.10 Schematic of circumferential pipe deformation 37

Figure 2.11A Sectioned diametral plane of a half liner in a simple model, radial

loading of the liner. p_{cp} is the contact pressure between the liner and the structural layers. 38

Figure 2.11B Sectioned diametral plane of half structural layers in a simple model, radial loading of the structural layers. p_{cp} is the internal pressure of the structural layers. 38

Figure 2.11C Transverse plane of a simple model (including the liner), axial loading of the liner and the structural layers. 39

Figure 2.12A Sectioned diametral plane of a half liner in a complex model, radial loading of the liner. p_{cp} is the contact pressure between the liner and the structural layers. 40

Figure 2.12B Sectioned diametral plane of half hoop layers in a complex model, radial loading of the hoop layers. p_{cp} is the contact pressure between the liner and the hoop layers, p_c is the pressure acting by the helix layers due to internal pressure of the pipe. 40

Figure 2.12C Sectioned diametral plane of half helix layers in a complex model, radial loading of the helix layers. p_c is the contact pressure between the hoop and helix layers. 41

Figure 2.12D Transverse plane of a complex model, axial loading of the liner and the structural layers. 41

Figure 4.1 End connection assembly of pipe "C" 62

Figure 5.1 Arrangement of strain gages on the load cell 68

Figure 5.2 Block diagram of the automatic control circuit for the cyclic pressure test 69

Figure 5.3 Timing diagram for the automatic control logic 70

Figure 5.4 Arrangement of the test apparatus in testing of pipe "C" 71

Figure 5.5 Rotating end with the isolating valve 72

Figure 5.6 Non-rotating end with the vent valve 73

Figure 6.1 The measurements of end connection domain, transition area and pipe domain 79

Figure 6.2 Relative position of the failed layers 80

Figure 6.3 Failure configuration of the hoop strips 81

Figure 6.4 Failure configuration of the helix strips 81

Figure 7.1 End connection assembly of pipe "D3" 87

List of Symbols

a_c	Coefficient of linear thermal expansion of the composite strips in simple model
a_e	Coefficient of linear thermal expansion of the helix layers
a_o	Coefficient of linear thermal expansion of the hoop layers
a_p	Coefficient of linear thermal expansion of the polymer liner
E_c	Tensile modulus of the composite strip material in simple model
E_e	Tensile modulus of the helix strip material
E_o	Tensile modulus of the hoop strip material
E_p	Young's modulus of the polymer liner material
F	Axial load applied to the pipe
F_{re}	Longitudinal resultant force acting on the pipe end
L	Length of a structural strips in one pitch of the structural wrap
δL	Small change in L
p	Internal pressure
p_c	Contact pressure between hoop layers and helix layers resulting from internal pressure
p_e	External pressure
p_t	Thermal contact pressure generated between structural layers and polymer liner resulting from temperature change
p_{cp}	Contact pressure between polymer liner and structural layers resulting from internal pressure
p_{ct}	Thermal contact pressure generated between hoop layers and helix layers resulting from temperature change
r	Nominal radius of the pipe
t_c	Radial thickness of each composite layer in simple model
t_e	Radial thickness of each helix layer
t_o	Radial thickness of each hoop layer
t_p	Radial thickness of polymer liner
T_e	Torque generated by a single helix layer
T_o	Torque generated by a single hoop layer

Z	Axial length in one pitch of structural wrap
δZ	Small change in Z
α	Volume fraction of structural material in structural layers of simple model
α_e	Volume fraction of structural composite material in helix layers
α_o	Volume fraction of structural composite material in hoop layers
$1-\alpha$	Volume fraction of elastomeric material in structural layers of simple model
$1-\alpha_e$	Volume fraction of elastomeric material in helix layers
$1-\alpha_o$	Volume fraction of elastomeric material in hoop layers
σ	Tensile stress in structural strips of simple model
σ_c	Thermal stress in composite strips of simple model
σ_e	Tensile stress in helix strips
σ_o	Tensile stress in hoop strips
σ_z	Longitudinal stress in polymer liner
σ_Θ	Circumferential stress in polymer liner
μ	Poisson's ratio of the polymer liner material
δT_c	Temperature change in structural layers of the simple model
δT_e	Temperature change in helix layers
δT_o	Temperature change in hoop layers
δT_p	Temperature change in polymer liner
ϕ	Helix angle of the structural strips relative to the pipe axis in simple model
ϕ_e	Helix angle of the helix strips relative to the pipe axis
ϕ_o	Helix angle of the hoop strips relative to the pipe axis
ε	Strain in composite strips of the simple model
ε_c	Total strain in composite strips of the simple model resulting from thermal effect
ε_e	Strain in helix strips
ε_o	Strain in hoop strips
ε_z	Longitudinal strain in the pipe
ε_Θ	Circumferential strain in the pipe

Chapter 1 Introduction

Flexible tubular structures investigated in this thesis are tubular products (pipe) capable of withstanding high internal pressure (similar to conventional steel pipe) but are flexible enough to be coiled into transportation spools. This is advantageous compared to conventional steel pipe since the structure can be manufactured in long continuous spans.

Risers used in offshore applications have to be flexible in order to accommodate floating platform motion and hydrodynamic loading. Hence, flexible pipe has an obvious advantage over rigid steel pipe in offshore application. The inland pipeline industry uses rigid steel pipes, which are heavy and thus costly to handle and transport. They are also susceptible to chemical deterioration and cyclic fatigue, and require skilled labour and time to weld or otherwise join in a field environment. A cost effective, corrosion-resistant, continuous and flexible pipe is a reliable, economical replacement for rigid steel pipe.

Flexible steel pipe can be either a bonded structure or unbonded structure. In a bonded structure, steel components are embedded in elastomeric materials to reduce steel to steel contact. It has an interlocking mechanism on the innermost structural layer to prevent the underlying polymer liner from extruding through the interstices under high internal pressure. In an unbonded structure different components are applied in individual layers and remain separated structurally allowing internal movement between layers. The first flexible steel pipe was placed in service in 1970s [1]. The major disadvantage of flexible steel pipe is its prohibitive cost in both manufacturing and operation due to its weight.

A low cost, unbonded, light weight flexible fibre reinforced composite pipe conforming to present performance standards is studied in this thesis for utilization in the pipeline industry. Continuous fibre reinforced composites are transversely isotropic and thus more efficient in resisting uniaxial stress induced under load in a flexible pipe than isotropic materials such as steel. Furthermore, composite materials are low modulus, light weight and continuous and thus ideally suitable for making a continuous flexible

tubular structure. The unique structural feature of this pipe is the construction of the wall in discrete helical strips which are loaded primarily in uniaxial tension along the strip. The pipe structure allows large deflections without significant bending stresses. It has high corrosion-resistance, is easy to handle and to coil into spools. The major applications are transportation of hydrocarbons, chemicals, water, oil and gas in both offshore and inland applications.

The behaviour of flexible composite pipe under different loading conditions was established prior to this study [2], in which the liner was ignored as a structural member. Feret [3] has modelled the flexible tubular structure including the axial force and internal pressure acting simultaneously. Feret also analyzed the deformation of the structure including axial strain, radial strain and shear strain simultaneously in the strain equations of the structural layers. Approximate formulas were presented in [3], in which the structural layers to resist radial force were assumed to be wound at 90°. Oliveira [4] studied the behaviour of flexible pipe including the collapse strength. Shear strain was not included in the strain equations of the structural layers in Oliveira's analysis. Numerical comparison between the theoretical results and the test results was also presented in [4]. The analysis presented by Goto [4] included the crushing strength of flexible pipe. Again, the comparison of the analytical results and the testing results were provided in [4].

Metallic structural layers of flexible pipe was considered in the analysis contributed by Feret, Oliveira and Goto. However, investigation including liner as a structural layer and thermal analysis was not done in their analyses. The contribution of the liner as a structural layer could be more significant in flexible composite pipe than in flexible steel pipe due to the lower modulus value of composite material. Thermal stress in the pipe are generated when the operation temperature of the pipe is different from the pipe manufacturing temperature. In addition to the elastic analysis of the liner and the investigation of thermally induced stresses in the pipe, end connection design is included in this thesis. Discussion and results of hydrostatic tests are also included in this thesis.

Chapter 2 Theory

This chapter will show the equilibrium condition for loading a simple helical structure by internal pressure. However, the equilibrium configuration is load dependent. This simple model identifies a helix angle which is useful in the more complex hoop/helix model developed next. In the hoop/helix model, equilibrium is easily achieved as long as one helix angle is less than and the other is greater than that identified in the simple model. Figure 2.1 shows the simple model configuration.

2.1 Simple model

In the simple model, the pipe is reinforced by two identical structural layers. One layer is wrapped with helix angle of angle ϕ and the other is wrapped with an angle $-\phi$. The structural strips are made of fibre-glass reinforced plastic, and the stress in the strips are parallel to the fibre direction. The polymer liner will then transfer all the load to the structural layers. Hence, all the load on the pipe is balanced by the stress induced in the structural strips. Elastomer strips, of very low elastic modulus are placed between the structural strips. These elastomer strips have no real purpose in the simple model, but allow this analysis and the symbols already defined to be consistent with the complex model.

The following are the assumptions used in the analysis of a simple model.

1. Each of two structural layers are of equal radial thickness.
2. Each structural layer is composed of structural strips of isotropic or transversely isotropic material, and elastomer strips.
3. The helix angle of each structural layer is the same but the hand is opposite.
4. The liner contains internal pressure but has a low elastic modulus and does not function as a structural layer.
5. The total radial thickness of the structural layers is much less than the pipe radius.
6. The structural strips of the structural layers are loaded in tension only.
7. The elastomer strips do not contribute structurally.

Critical angle

Consider the simple helix/hoop model as an enclosed pressure vessel with unrestrained ends. Internal pressure (p) acts on the projected area of the pipe (πr^2) at the pipe end and produces a longitudinal force on the pipe. This longitudinal force is balanced by the induced tensile stress in the structural strips. The longitudinal force equilibrium equation (see the free body diagram in figure 2.2A) of the pipe is expressed as

$$\pi r^2 p = 4\pi r t_c \alpha \sigma \cos^2\phi$$

or

$$p = \frac{4\sigma t_c \alpha \cos^2\phi}{r} .$$

Therefore

$$\sigma = \frac{pr}{4\alpha t_c \cos^2\phi} , \qquad (2.1)$$

where σ is the tensile stress in the structural strips, t_c is the radial thickness of each structural strip, and α is the volume fraction of the structural material in the structural layers.

Similarly, the radial force on the pipe resulting from the internal pressure is balanced by the stress in the structural strips. The radial force equilibrium equation (see the free body diagram in figure 2.2B) per unit length of the pipe can be expressed as

$$2rp = 4t_c \alpha \sigma \sin^2\phi$$

or

$$p = \frac{2\sigma \alpha t_c \sin^2\phi}{r} .$$

Therefore

$$\sigma = \frac{pr}{2\alpha t_c \sin^2\phi} \quad . \tag{2.2}$$

Each structural strip of the pipe functions like a string in tension. Equations 2.1 and 2.2 result from separate equilibrium conditions for the model. Since there can be only one level of stress in the structural strips,

$$\frac{pr}{2t_c \alpha \sin^2\phi} = \frac{pr}{4t_c \alpha \cos^2\phi} \quad . \tag{2.3}$$

Solving equation 2.3 gives a critical angle for ϕ, which is 54.7°. This is the required orientation of the strips so that there is no movement of the pipe, under internal pressure, either in the longitudinal direction or in the radial direction. When the wrap angle is greater than the critical angle, the internal pressure will cause the wrap angle to decrease until the wrap becomes 54.7°. On the other hand, the helix angle will be increased by internal pressure until it becomes 54.7°. However, this critical angle is only valid for a capped end, otherwise equation 2.1 cannot apply.

2.2 Complex model

The complex model, which is shown in figure 2.3, consists of four structural layers of pipe reinforcement. Two have identical helix angles greater than 54.7° called hoop layers. Two have helix angles less than 54.7° and are called helix layers. Figure 2.4 shows the configuration of a hoop layer and figure 2.5 shows the configuration of a helix layer. Similar to the simple model, the helix angles of the hoop layers are of opposite hand, as are the helix layers. The assumptions in section 2.1 are also applicable to the following investigations. The following discussions describe the behaviour of the pipe under different loading conditions. Both unrestrained end and restrained end are discussed below. The hoop layers can be placed inside or outside the helix layers.

Unrestrained end

In an unrestrained capped end pipe, the pipe is allowed to expand axially when the pipe is under load. The behaviour of the pipe under internal pressure, external pressure and axial tension is discussed below.

Internal pressure of unrestrained pipe

In order to understand the behaviour of the hoop and helix layers, the contact pressure between these two layers has to be considered. When the pipe is under internal pressure p, the net pressure acting on the hoop layers is $p-p_c$, where p_c is the contact pressure between the hoop and helix layers. Equation 2.2 is the expression of the equilibrium between the radial force acting on the pipe by the internal pressure and the stress induced in the structural strips. From similar equilibrium considerations (see the free body diagram in figures 2.6A, 2.6B and 2.6C), the stresses in the hoop and helix strips caused by internal pressure can be expressed as

$$\sigma_o = \frac{(p-p_c)\,r}{2t_o\alpha_o \sin^2\phi_o} \qquad (2.4)$$

and

$$\sigma_e = \frac{p_c r}{2t_e \alpha_e \sin^2\phi_e} \quad . \tag{2.5}$$

When the pipe is under internal pressure, the axial force equilibrium is

$$\pi r^2 p = 4\pi r t_o \alpha_o \sigma_o \cos^2\phi_o + 4\pi r t_e \alpha_e \sigma_e \cos^2\phi_e \quad . \tag{2.6}$$

σ_o and σ_e of equations 2.4 and 2.5 can be substituted into equation 2.6 to obtain the expression for p_c,

$$p_c = p\frac{1/2 - \cot^2\phi_o}{\cot^2\phi_e - \cot^2\phi_o} \quad . \tag{2.7}$$

Equation 2.7 is the expression of the contact pressure due to internal pressure on a unrestrained capped end pipe.

External pressure of unrestrained pipe

When the pipe is under external pressure (p_e), equations 2.4 and 2.5 can be written as

$$\sigma_o = \frac{-p_c r}{2t_o \alpha_o \sin^2\phi_o} \tag{2.8}$$

and

$$\sigma_e = \frac{-(p_e - p_c)}{2t_e \alpha_e \sin^2\phi_e} \quad . \tag{2.9}$$

The axial force equilibrium equation for the pipe when the pipe is under external pressure is

$$-p_e \pi r^2 = 4\sigma_o \pi r t_o \alpha_o \cos^2\phi_o + 4\sigma_e \pi r t_e \alpha_e \cos^2\phi_e \quad . \tag{2.10}$$

After solving the above three expressions, it gives the expression of p_c due to external pressure,

$$p_c = p_e \frac{1/2 - \cot^2\phi_e}{\cot^2\phi_o - \cot^2\phi_e} \quad . \tag{2.11}$$

Axial tension on unrestrained pipe

At equilibrium condition, when the pipe is under axial tension (F), the helix layers develop a tensile stress and contract radially onto the hoop layers, which introduces contact pressure between the hoop and helix layers. The axial force equilibrium equation is expressed as

$$F = 4\sigma_o \pi r t_o \alpha_o \cos^2\phi_o + 4\sigma_e \pi r t_e \alpha_e \cos^2\phi_e \quad . \tag{2.12}$$

Equations 2.4 and 2.5 are useful in expressing the stresses in the structural layers. However, p in equation 2.5 is zero for no internal pressure in the pipe. By substituting the expressions for σ_o and σ_e into equation 2.12,

$$p_c = \frac{F}{2\pi r^2 (\cot^2\phi_e - \cot^2\phi_o)} \quad . \tag{2.13}$$

Equation 2.13 is the expression for the contact pressure when the pipe is under axial tension.

Torsion due to internal pressure of unrestrained pipe

The following analysis deals with torsional loading resulting from internal pressure. For symmetric configuration, where there are right hand and left hand strips of equal thickness, there will be no torsion generated. The torque (T_o) generated by a single hoop layer is

$$T_o = 2\sigma_o \pi r^2 t_o \alpha_o \cos\phi_o \sin\phi_o \quad . \tag{2.14}$$

This relationship can be obtained from figure 2.7.

Substituting equation 2.4 into σ_o of equation 2.14 results in

$$T_o = 2\pi r^3 (p - p_c) \cot\phi_o \ . \qquad (2.15)$$

Similarly, the torque generated by a single helix layer is expressed as:

$$T_e = 2\pi r^3 p_c \cot\phi_e \ . \qquad (2.16)$$

Pipe deformation

When the pipe is loaded, by internal pressure or by axial tension, the strains along the fibre in each of the hoop and helix layers are different due to the differences in geometry of the two layers. For either loading, the circumferential strain is assumed to be the same for both hoop and helix layers. This assumption also applies to the longitudinal strain. The following analysis obtains the compatibility equations relating hoop and helix fibre strain to axial and circumferential strain of the pipe.

To illustrate the strain in the composite strips, a helically wound strip including one pitch of helix has length L, and which wraps once around the pipe at wrap angle ϕ (see figures 2.8A and 2.8B) is considered.

Figure 2.9 relates the change in length of the composite strip to elongation of the pipe in the longitudinal direction. From figure 2.9, the increase in length of the composite strips due to longitudinal elongation of the pipe is equal to δL.
From figure 2.9, it is clear that

$$Z = L\cos\phi \ ,$$

where Z is the axial length of one pitch of the structural wrap.
Also from figure 2.9, referring to the components of axial growth δZ,

$$\delta L = \delta Z \cos\phi \ .$$

Then

$$\delta Z = \frac{\delta L}{\cos\phi} = \frac{\varepsilon L}{\cos\phi} = \frac{\varepsilon}{\cos\phi}\frac{Z}{\cos\phi} \ .$$

where ε is the strain in the composite strip, and

$$\frac{\delta Z}{Z} = \varepsilon_z = \frac{\varepsilon}{\cos^2\phi} ,$$

or

$$\varepsilon = \varepsilon_z \cos^2\phi . \qquad (2.17)$$

Figure 2.10 relates the increase in length of the composite strip to circumferential growth of the pipe. δL is the change in length of the composite strip. The component of circumference change which is aligned with the strip is

$$\delta L = \delta(2\pi r)\sin\phi .$$

Also,

$$2\pi r = L\sin\phi .$$

Then

$$\frac{\delta L}{2\pi r} = \frac{\delta(2\pi r)\sin\phi}{2\pi r} = \frac{\delta L}{L\sin\phi} .$$

Therefore

$$\frac{\delta L}{L} = \frac{\delta(2\pi r)\sin^2\phi}{2\pi r} ,$$

or

$$\varepsilon = \varepsilon_\theta \sin^2\phi . \qquad (2.18)$$

Assuming small strains and using equations 2.17 and 2.18, the total strain ε of the composite strip is given as

$$\varepsilon = \varepsilon_z \cos^2\phi + \varepsilon_\theta \sin^2\phi . \qquad (2.19)$$

Equation 2.19 relates the pipe strain to the longitudinal strain and circumferential strain in the structural layers.

From equations 2.4 and 2.5, the strain of hoop strip ε_o and strain of helix strip ε_e can be written as

$$\varepsilon_o = \frac{\sigma_o}{E_o} = \frac{(p-p_c)r}{2t_o\alpha_o E_o \sin^2\phi_o} \tag{2.20}$$

and

$$\varepsilon_e = \frac{\sigma_e}{E_e} = \frac{p_c r}{2t_e\alpha_e E_e \sin^2\phi_e} \ . \tag{2.21}$$

Combining equations 2.20 and 2.21 with the expression of ε_z and ε_Θ, it gives

$$\varepsilon_o = \frac{(p-p_c)r}{2t_o\alpha_o E_o \sin^2\phi_o} = \varepsilon_z \cos^2\phi_o + \varepsilon_\theta \sin^2\phi_o \tag{2.22}$$

and

$$\varepsilon_e = \frac{p_c r}{2t_e\alpha_e E_e \sin^2\phi_e} = \varepsilon_z \cos^2\phi_e + \varepsilon_\theta \sin^2\phi_e \ . \tag{2.23}$$

By solving ε_z and ε_Θ from the equations 2.22 and 2.23, it gives

$$\varepsilon_z = \frac{\dfrac{(p-p_c)r\sin^2\phi_e}{2t_o\alpha_o E_o \sin^2\phi_o} - \dfrac{p_c r \sin^2\phi_o}{2t_e\alpha_e E_e \sin^2\phi_e}}{\cos^2\phi_o \sin^2\phi_e - \cos^2\phi_e \sin^2\phi_o} \tag{2.24}$$

and

$$\varepsilon_\theta = \frac{\dfrac{p_c r\cos^2\phi_o}{2t_e\alpha_e E_e \sin^2\phi_e} - \dfrac{(p-p_c)r\cos^2\phi_e}{2t_o\alpha_o E_o \sin^2\phi_o}}{\cos^2\phi_o \sin^2\phi_e - \cos^2\phi_e \sin^2\phi_o} \tag{2.25}$$

From the equations 2.24, it is possible to have any desired longitudinal pipe deformation. The condition for zero longitudinal pipe growth when the pipe is under internal pressure is

$$\frac{(p-p_c)r\sin^2\phi_e}{2t_o\alpha_o E_o \sin^2\phi_o} - \frac{p_c r \sin^2\phi_o}{2t_e\alpha_e E_e \sin^2\phi_e} = 0 \ .$$

From equation 2.7, contact pressure for the pipe with capped and unrestrained ends was shown to be

$$p_c = p\frac{1/2-\cot^2\phi_o}{\cot^2\phi_e-\cot^2\phi_o} \ .$$

Therefore, for zero longitudinal strain,

$$\frac{t_o}{t_e} = \frac{(\cot^2\phi_e-1/2)}{(1/2-\cot^2\phi_o)}\frac{\sin^4\phi_e}{\sin^4\phi_o}\frac{\alpha_e E_e}{\alpha_o E_o} \ . \qquad (2.26)$$

Therefore E_e, E_o, α_e, α_o, t_e, t_o, ϕ_e or ϕ_o can be carefully selected to obtain zero longitudinal strain of the pipe, for arbitrary internal pressure.

Restrained ends

With restrained ends, a more common case when a pipe is in service, the axial strain of the pipe is zero. The stresses developed in the hoop layers and the helix layers for this condition are discussed in the following sections. The major difference in behaviour of a unrestrained end pipe and a restrained end pipe is the contact pressure between the hoop and helix layers.

Contact pressure of restrained pipe

Since the pipe is restrained, the axial strain of the pipe is zero. From equation 2.24, the expression of axial strain is written as

$$\varepsilon_z = 0 = \frac{\dfrac{(p-p_c)r\sin^2\phi_e}{2t_o\alpha_o E_o \sin^2\phi_o} - \dfrac{p_c r \sin^2\phi_o}{2t_e\alpha_e E_e \sin^2\phi_e}}{\cos^2\phi_o\sin^2\phi_e-\cos^2\phi_e\sin^2\phi_o}$$

or

$$p_c = \frac{p\sin^4\phi_e t_e \alpha_e E_e}{\sin^4\phi_o t_o \alpha_o E_o + \sin^4\phi_e t_e \alpha_e E_e} \quad . \tag{2.27}$$

It is noteworthy that the expression of the contact pressure is different for unrestrained ends than for restrained ends. However, the contact pressure in the unrestrained pipe is the same as that in the restrained pipe if the pipe was designed for zero axial growth. From equation 2.26

$$\frac{t_o}{t_e} = \frac{(\cot^2\phi_e - 1/2)}{(1/2 - \cot^2\phi_o)} \frac{\sin^4\phi_e}{\sin^4\phi_o} \frac{\alpha_e E_e}{\alpha_o E_o} \quad .$$

Therefore, substituting for t_o results in equation 2.27, it gives

$$p_c = p \frac{\sin^4\phi_e t_e \alpha_e E_e}{\sin^4\phi_o t_e \frac{(\cot^2\phi_e - 1/2)}{(1/2 - \cot^2\phi_o)} \frac{\sin^4\phi_e}{\sin^4\phi_o} \frac{\alpha_e E_e}{\alpha_o E_o} (\alpha_o E_o) + \sin^4\phi_e t_e \alpha_e E_e} \quad .$$

After some simplification, the result become

$$p_c = \frac{p(1/2 - \cot^2\phi_o)}{\cot^2\phi_e - \cot^2\phi_o} \quad .$$

Therefore, in this particular condition, p_c is expressed as

$$p_c = \frac{p(1/2 - \cot^2\phi_o)}{\cot^2\phi_e - \cot^2\phi_o} = \frac{p\sin^4\phi_e t_e \alpha_e E_e}{\sin^4\phi_o t_o \alpha_o E_o + \sin^4\phi_e t_e \alpha_e E_e} \quad . \tag{2.28}$$

Stresses in structural layers of restrained pipe

Any change in contact pressure can be related to a change in stresses in the structural layers. The expressions in equations 2.4 and 2.5 are equilibrium expressions from radial load consideration which are valid for any pipe loading including restrained ends. These two equations are not affected by the loading condition of the pipe in the

longitudinal direction, and they can be applied to either a capped or an un-capped end pipe. After including the appropriate expressions for contact pressure given by equation 2.27 and re-arranging equations 2.4 and 2.5, the expressions of the stresses in hoop layers and the helix layers for the restrained ends condition are

$$\sigma_o = \frac{pr\sin^2\phi_c E_o}{2(\sin^4\phi_o t_o \alpha_c E_o + \sin^4\phi_c t_c \alpha_c E_c)} \tag{2.29}$$

and

$$\sigma_c = \frac{pr\sin^2\phi_c E_c}{2(\sin^4\phi_o t_o \alpha_c E_o + \sin^4\phi_c t_c \alpha_c E_c)} \ . \tag{2.30}$$

Circumferential strain of restrained pipe

The expression of circumferential strain in equation 2.25 is applicable to both unrestrained and restrained pipe. However, the expression of p_c in equation 2.27 is only valid for restrained pipe. Therefore, the circumferential strain ε_θ in restrained pipe can be obtained by substituting p_c of equation 2.27 into equation 2.25.

2.3 Stress analysis including behaviour of the liner

The stiffness of the polymer liner was assumed to be zero in the above analysis. This assumption was made for two reasons. The elastic modulus of a typical liner material (high density polyethylene, tensile modulus of 145,000 psi) is considerably lower than that of composite (polyester - E-glass, tensile modulus of 3.5×10^6 psi). On this basis, the liner accounts for a small fraction of the pipe load when initially applied. Secondly, due to the phenomenon of creep, the load relaxation characteristics of materials such as polyethylene results in the eventual load transfer from the liner to the composite structure. The following is a discussion of the stress analysis including the structural contribution of the liner. This analysis accounts for the structural characteristics of the pipe after initial load application.

This analysis is necessary for subsequent thermal analysis of flexible tubular structures. Viscoelastic modelling is not included in this analysis. Instead, only elastic modelling of the liner is considered. The modulus of the liner is allowed to decrease to zero. In this simple manner, load relaxation of the liner is approximated.

Internal pressure of simple model

The simple model has the same composite structure as that mentioned in section 2.1 but includes a liner on the inside of this structure. For this model, a free body diagram of the liner is shown in figure 2.11A, a free body diagram of the composite structure is shown in figure 2.11B and a free body diagram of the combined structure is shown in figure 2.11C. For radial force equilibrium, the hoop stress in the liner is

$$\sigma_\theta = \frac{(p-p_{cp})r}{t_p} , \qquad (2.31)$$

where p_{cp} is contact pressure between the liner and the structural layers resulting from internal pressure.

The axial force on the pipe produced by internal pressure is balanced by the stresses induced in the liner and the composite strips (see figure 2.11C). Axial force equilibrium is only applicable in an unrestrained end pipe and is determined by

$$\pi r^2 p = 2\pi r t_p \sigma_z + 2\pi r t_c \alpha \sigma \cos^2\phi$$

or

$$pr = 2\sigma_z t_p + 2\sigma t_c \alpha \cos^2\phi \tag{2.32}$$

where t_p is the thickness of the liner and σ_z is the axial stress in the liner.

Similarly to equation 2.4, the stress induced in the structural layers is

$$\sigma = \frac{p_{cr} r}{2 t_c \alpha \sin^2\phi} \ . \tag{2.33}$$

Using Hooke's law, the hoop strain and longitudinal strain in the liner relate to hoop stress and longitudinal stress

$$\varepsilon_\theta = \frac{\sigma_\theta}{E_p} - \mu \frac{\sigma_z}{E_p} \tag{2.34}$$

and

$$\varepsilon_z = \frac{\sigma_z}{E_p} - \mu \frac{\sigma_\theta}{E_p} \ , \tag{2.35}$$

where E_p is the tensile modulus of the liner and μ is the Poisson's ratio of the liner material. ε_θ is the circumferential strain of the pipe and ε_z is the axial strain of the pipe.

The strain in the structural layer relates the stress in the structural layers to the tensile modulus of the structural layers

$$\varepsilon_c = \frac{p_{cr} r}{2 t_c \alpha E_c \sin^2\phi} \ . \tag{2.36}$$

Equation 2.19 relates the axial strain and circumferential strain of the pipe to the strain in the structural layer. This expression is also applied in this analysis, then

$$\varepsilon = \varepsilon_z \cos^2\phi + \varepsilon_\theta \sin^2\phi \ . \tag{2.37}$$

Restrained ends

In the case of a restrained end pipe, the axial strain of the pipe is zero ($\varepsilon_z = 0$). Equations 2.31 to 2.37 are applicable except equation 2.32, because an external force is required to obtain the axial force equilibrium on the pipe. There are then six unknowns in this analysis, they are σ_θ, σ_z, σ, ε_θ, ε, and p_{cp}. After solving these simultaneous equations, the expression of p_{cp} is

$$p_{cp} = p\frac{(1-\mu^2)\sin^2\phi}{(1-\mu^2)\sin^2\phi - \dfrac{E_p t_p}{2t_c \alpha E_c \sin^2\phi}} . \qquad (2.38)$$

When the liner undergoes load relaxation, that is when E_p becomes very small, the contact pressure between the liner and the structural layers (p_{cp}) will be equal to the internal pressure of the pipe (p). The expressions of the other unknowns can be obtained by substituting p and p_{cp} into the equations 2.31 to 2.37 except equation 2.32.

Unrestrained ends

All the above equations for simple pipe model are applicable for unrestrained ends. Therefore, there are seven equations and seven unknowns. The unknowns are σ_θ, σ_z, σ, ε_θ, ε_z, ε, and p_{cp}. Solving equations 2.31 to 2.37 simultaneously, it gives the expression of p_{cp} as

$$p_{cp} = p\frac{(1+2\mu)\cos^2\phi - (2+\mu)\sin^2\phi}{\dfrac{E_p t_p}{t_c \alpha E_c \sin^2\phi} + (2\mu + 2\cot^2\phi)\cos^2\phi - (2+2\mu\cot^2\phi)\sin^2\phi} .$$

(2.39)

For very small values of the liner modulus, p equal to p_{cp}. However, this requires the helix angle of the structural layers become 54.7°. This will happen since the model becomes identical with that discussed in section 2.1.

Axial tension of simple model

When the simple model pipe is under axial tension F, the axial force equilibrium

between the applied force and the stresses induced in the liner and the structural layers is expressed as

$$F = 2\pi r t_p \sigma_z + 4\pi r t_c \alpha \cos^2\phi \sigma \ . \qquad (2.40)$$

Equations 2.31 to 2.37 are applicable in the case of axial tension except equation 2.32. Therefore, there are seven equations with seven unknowns, the unknowns are p_{cp}, σ, σ_θ, σ_z, ε, ε_θ, and ε_z. After solving these equations,

$$F = 2\pi r^2 p_{cp} \left[\frac{E_p t_p}{\cos^2\phi - \mu \sin^2\phi} \left(\frac{1}{2 t_c \alpha E_c \sin^2\phi} + \frac{\sin^2\phi - \mu\cos^2\phi}{E_p t_p} \right) + \cot^2\phi \right] . \qquad (2.41)$$

When the liner exhibits load relaxation, the modulus of the liner becomes very small. The contact pressure between the liner and the structural layers will disappear, all the axial tension will then transfer to the structural layers. In such a condition, the helix angle of the structural layers will go to zero.

Internal pressure of complex model

The complex model configuration is the same as mentioned in section 2.2. The following discussions describe both unrestrained ends pipe and restrained ends pipe. Hoop stress and longitudinal stress are developed in the liner when internal pressure is applied to the pipe. Due to radial expansion of the liner under internal pressure, contact pressure will be developed between the liner and the structural layers. This causes the tensile stresses in the hoop and helix layers.

Free body diagrams for the liner, hoop structure, helix structure and for the entire pipe structure are shown in figure 2.12A, 2.12B, 2.12C and 2.12D respectively, where the liner is the innermost layer and the helix structure is the outermost structure of the pipe.

For circumferential force equilibrium, the hoop stress in the liner is related to the pressure difference between the inner and outer surfaces of the liner. The expression of

this hoop stress in the liner is

$$\sigma_\theta = \frac{(p-p_{cp})r}{t_p} \quad . \tag{2.42}$$

The longitudinal force due to internal pressure acting on the projected area at the end of the pipe is balanced by the stress on the hoop and helix layers and the longitudinal stress in the polymer liner. If the ends are unrestrained, the equilibrium equation for this longitudinal force is

$$\pi r^2 p = 4\sigma_o \pi r t_o \alpha_o \cos^2\phi_o + 4\sigma_e \pi r t_e \alpha_e \cos^2\phi_e + 2\pi r t_p \sigma_z$$

or

$$pr = 4\sigma_o t_o \alpha_o \cos^2\phi_o + 4\sigma_e t_e \alpha_e \cos^2\phi_e + 2t_p \sigma_z \quad . \tag{2.43}$$

Using Hooke's Law, the hoop strain and longitudinal strain in the liner relate to hoop stress and longitudinal stress in the liner

$$\varepsilon_\theta = \frac{\sigma_\theta}{E_p} - \mu\frac{\sigma_z}{E_p} \tag{2.44}$$

and

$$\varepsilon_z = \frac{\sigma_z}{E_p} - \mu\frac{\sigma_\theta}{E_p} \quad . \tag{2.45}$$

The stress developed in the structural layers relates to the internal pressure and the contact pressure as mentioned in section 2.2. Now, the pressure between the liner and the hoop layers is p_{cp}, whilst the contact pressure between hoop and helix layers is p_c. Therefore, comparing the equations 2.4 and 2.5, the stresses in the hoop and helix layers are

$$\sigma_o = \frac{(p_{cp}-p_c)r}{2t_o \alpha_o \sin^2\phi_o} \tag{2.46}$$

and

$$\sigma_e = \frac{p_c r}{2t_e \alpha_e \sin^2\phi_e} \quad . \tag{2.47}$$

The strain in the structural strips relates to the tensile modulus of the structural strips. It can be expressed as

$$\varepsilon_o = \frac{\sigma_o}{E_o} = \frac{(p_{cp}-p_c)}{2t_o \alpha_o E_o \sin^2\phi_o} \tag{2.48}$$

and

$$\varepsilon_e = \frac{\sigma_e}{E_e} = \frac{p_c r}{2t_e \alpha_e E_e \sin^2\phi_e} \quad . \tag{2.49}$$

Equations 2.22 and 2.23 are used to relate the circumferential strain and axial strain of the pipe to the strain of the hoop layer and the helix layer. These two equations are applicable in this analysis to define the compatibility of the pipe and the structural layers. Therefore, there is a pair of compatibility equations, which are expressed as

$$\varepsilon_o = \varepsilon_\theta \sin^2\phi_o + \varepsilon_z \cos^2\phi_o \tag{2.50}$$

and

$$\varepsilon_e = \varepsilon_\theta \sin^2\phi_e + \varepsilon_z \cos^2\phi_e \quad . \tag{2.51}$$

Unrestrained ends

The pipe is free to expand in an unrestrained ends condition. Therefore, using the equations 2.42 to 2.51, there are ten independent equations and ten unknowns. The unknowns are p_c, p_{cp}, σ_θ, σ_z, ε_θ, ε_z, σ_o, σ_e, ε_o and ε_e. Once the unknowns p_c and p_{cp} are found, the other unknowns can be obtained by direct substituting p_{cp} and p_c into the equations 2.42 to 2.51. After solving these ten simultaneous equations, p_c and p_{cp} are found to be

$$p_{cp}=\frac{p(B-D)}{B-D+A}+\frac{p(A+C)}{B-D+A}\,\frac{\dfrac{A(B-D)}{B-D+A}-B+\dfrac{B(B-D)}{B-D+A}-\dfrac{1}{2E_pt_p}+\dfrac{B-D}{B-D+A}\dfrac{\cot^2\phi_o}{E_pt_p}}{A\left(1-\dfrac{A+C}{B-D+A}\right)-\dfrac{A+C}{B-D+A}\left(B+\dfrac{\cot^2\phi_o}{E_pt_p}\right)-\dfrac{\cot^2\phi_e-\cot^2\phi_o}{E_pt_p}} \tag{2.52}$$

and

$$p_c=p\,\frac{\dfrac{A(B-D)}{B-D+A}-B+\dfrac{B(B-D)}{B-D+A}-\dfrac{1}{2E_pt_p}+\dfrac{B-D}{B-D+A}\dfrac{\cot^2\phi_o}{E_pt_p}}{A\left(1-\dfrac{A+C}{B-D+A}\right)-\dfrac{A+C}{B-D+A}\left(B+\dfrac{\cot^2\phi_o}{E_pt_p}\right)-\dfrac{\cot^2\phi_e-\cot^2\phi_o}{E_pt_p}}\,, \tag{2.53}$$

where

$$A=\frac{1}{2t_o\alpha_oE_o\sin^2\phi_o}\,\frac{1}{\cos^2\phi_o-\mu\sin^2\phi_o}\,,$$

$$B=\frac{\sin^2\phi_o-\mu\cos^2\phi_o}{E_pt_p(\cos^2\phi_o-\mu\sin^2\phi_o)}\,,$$

$$C=\frac{1}{2t_e\alpha_eE_e\sin^2\phi_e}\,\frac{1}{\cos^2\phi_e-\mu\sin^2\phi_e}\,,$$

and

$$D=\frac{\sin^2\phi_e-\mu\cos^2\phi_e}{E_pt_p(\cos^2\phi_e-\mu\sin^2\phi_e)}\,.$$

It can be shown that p_{cp} in equation 2.52 is equal to p when E_p is very small or tends to zero. This is the case when the liner undergoes load relaxation. It is interesting to note that the pressure acting inside from the structural layers is equal to the internal

pressure when the liner experiences load relaxation, which is one of the assumptions in section 2.1. The contact pressure between the hoop and helix structures (p_c) in equation 2.53 also reduces to the value previously derived in section 2.2 when the liner modulus reduces to zero.

Restrained ends

In the case of a restrained end, the axial strain ε_z is zero. Equations 2.42 to 2.51 are still applicable except equation 2.43, which is the equilibrium equation of longitudinal force. Because the ends of the pipe are restrained, the axial force on the pipe is not in equilibrium without an external force. Equations 2.42 to 2.51 should be modified by substituting $\varepsilon_z = 0$ and removing equation 2.43. Thus, the expressions of the contact pressures p_{cp} and p_c can be obtained by solving the modified equations simultaneously. Therefore, there become nine equations and nine unknowns for the complex pipe model, the unknowns for these simultaneous equations are σ_o, σ_c, ε_o, ε_c, σ_Θ, σ_z, ε_Θ, p_{cp} and p_c. After solving the equations simultaneously, the expressions of p_{cp} and p_c become

$$p_{cp} = \frac{p(N\sin^2\phi_o + \frac{EN}{G}\sin^2\phi_c)}{E + \frac{EN}{G}\sin^2\phi_c + N\sin^2\phi_o} \tag{2.54}$$

and

$$p_c = \frac{p\frac{EN}{G}\sin^2\phi_c}{N\sin^2\phi_o + \frac{EN}{G}\sin^2\phi_c + E}\ , \tag{2.55}$$

where

$$E = \frac{1}{2t_o\alpha_o E_o \sin^2\phi_o}\ ,$$

$$N = \frac{1-\mu^2}{E_p t_p} ,$$

and

$$G = \frac{1}{2t_c \alpha_c E_c \sin^2\phi_c} .$$

Again p_{cp} in equation 2.54 is equal to p when E_p becomes very small. This is the case for the liner experiencing load relaxation. In such a case, the pressure acting on the liner will be transferred to the structural layers. The contact pressure between the hoop and helix layer (p_c) in equation 2.55 also becomes the same value derived in section 2.2 when the liner modulus becomes zero.

Axial force of complex model

The structural layers will expand axially and contract radially when the pipe is loaded by an axial force. Hence, contact pressure between the liner and structural layers will be developed. The contact pressure between the liner and the hoop layers is an external pressure acting on the liner and compressive hoop stress will be developed in the liner, and may be developed in the hoop structure. Buckling due to these compressive stresses is not considered in this thesis. The expression for the hoop stress in the liner is

$$\sigma_\theta = -\frac{p_{cp} r}{t_p} . \qquad (2.56)$$

Similar to the condition of internal pressure, the axial force applied to the pipe is balanced by the stresses in the hoop layers and helix layers and the longitudinal stress in the liner. The equilibrium equation for the axial force is

$$F = 2\pi r t_p \sigma_z + 4\pi r t_c \alpha_c \cos^2\phi_c \sigma_c + 4\pi r t_o \alpha_o \cos^2\phi_o \sigma_o . \qquad (2.57)$$

Using the additional equations of hoop stress in the liner and axial force equilibrium equation above, and the equations 2.44 to 2.51, there are ten equations and

ten unknowns, the unknowns are p_c, p_{cp}, σ_θ, σ_z, ε_θ, ε_z, σ_o, σ_c, ε_o, and ε_c. The contact pressures, p_c and p_{cp}, are obtained first and the other unknowns can be obtained by direct substitution of p_c and p_{cp} into the respective equations.

After solving these ten equations simultaneously, it gives

$$p_{cp} = \frac{F(P+Q)}{2\pi r^2[(PR+PS+QR)E_p t_p + (R+S-Q)\cot^2\phi_c + (P+Q-S)\cot^2\phi_o]} \tag{2.58}$$

and

$$p_c = \frac{F(R+S-Q)}{2\pi r^2[(PR+PS+QR)E_p t_p + (R+S-Q)\cot^2\phi_c + (P+Q-S)\cot^2\phi_o]} , \tag{2.59}$$

where

$$P = \frac{1}{2t_c\alpha_c E_c \sin^2\phi_c}\frac{1}{\cos^2\phi_c - \mu\sin^2\phi_c} ,$$

$$Q = \frac{\sin^2\phi_c - \mu\cos^2\phi_c}{E_p t_p(\cos^2\phi_c - \mu\sin^2\phi_c)} ,$$

$$R = \frac{1}{2t_o\alpha_o E_o \sin^2\phi_o}\frac{1}{\cos^2\phi_o - \mu\sin^2\phi_o} ,$$

and

$$S = \frac{\sin^2\phi_o - \mu\cos^2\phi_o}{E_p t_p(\cos^2\phi_o - \mu\sin^2\phi_o)} .$$

Equation 2.59 will become the same as equation 2.13 when E_p is very small. Also, when E_p is very small, p_{cp} will become zero. Again, this corresponds to the physical condition when the liner undergoes load relaxation. The contact pressure (p_c) in equation 2.59 also reduces to the expression derived earlier when the liner was ignored.

2.4 Prototype design

A prototype called pipe "C", was developed to verify the equations developed in section 2.2 of this chapter. The pipe was designed to have zero axial strain and zero rotation under internal pressure of unrestrained ends condition. The total length of the pipe from flange to flange was twenty one feet. The length of each end connection was twenty four inches. Pipe "C" was composed of a liner, two hoop layers and two helix layers. The polymer liner was made of high density polyethylene (HDPE). Each structural layer had composite strips separated with elastomer strips. The composite strips were composed of 70% in volume of E-glass in a polyester matrix. The elastomer strips were made of flexible polyvinyl chloride (PVC). The innermost and the outermost structural layers were the hoop layers, and the two helix layers were in the middle. An anti-friction polyethylene film with thickness of two thousandth of an inch was wrapped in between every two adjacent structural layers. The designed physical parameters of the prototype are listed in table 2.1.

Table 2.1
Designed parameters of the pipe "C"

LAYER	I.D.	THICKNESS	O.D.	α	ϕ	NO. OF STRIPS	HAND
Liner	2.892"	0.204"	3.3"				
Inner Hoop	3.3"	0.06"	3.42"	67.5%	60.66°	2	Left
Inner Helix	3.42"	0.06"	3.54"	48.9%	30.09°	10	Right
Outer Helix	3.54"	0.06"	3.66"	48.9%	30.09°	13	Left
Outer Hoop	3.66"	0.06"	3.78"	67.5%	60.66°	6	Right

Despite the best attempt to produce the prototypes as designed, it was found that the dimensions given in table 2.2 were what was actually produced. The differences

between the designed and the manufactured prototype are helix angles for hoop and helix layers, thickness of structural layers, and volume fractions of the structural material in structural layers.

Table 2.2
Manufactured parameters of pipe "C"

LAYER	I.D.	THICKNESS	O.D.	α	ϕ	NO. OF STRIPS	HAND
Liner	2.892"	0.204"	3.3"				
Inner Hoop	3.3"	0.075"	3.45"	70.0%	60.77°	2	Left
Inner Helix	3.45"	0.065"	3.58"	54.1%	29.11°	10	Right
Outer Helix	3.58"	0.06"	3.70"	51.5%	29.17°	13	Left
Outer Hoop	3.70"	0.06"	3.82"	65.6%	60.91°	6	Right

Five thousand psi internal pressure was the design pressure of the pipe based on the hoop layers of the pipe attaining the ultimate strength. The equations derived from section 2.2 were unot sed to predict the behaviour of the structural layers. Equations 2.4 and 2.5 were used to calculate the stresses in the hoop layer and the helix layer in unrestrained capped ends of the pipe. Equations 2.29 and 2.30 were used in calculating the stresses in hoop and helix layers of restrained ends pipe. Equations 2.24 and 2.25 were used to obtain the axial strain and circumferential strain respectively of the pipe at 5,000 psi. Equations 2.24 and 2.25 are applicable for both unrestrained and restrained end tests. Nominal radius of the pipe, which was one and a half inches, was used for the radius r in these equations. The net torque generated on pipe "C" should always be zero due to the balanced configuration of the prototype. A zero net torque pipe should generate zero rotation when the pipe is under internal pressure. The design parameters of the prototype were used in the calculations of the stresses in the structural layers and the strains of the pipe, the results of the calculations are shown in table 2.3. The calculated results based on the manufactured parameters were included in the

calculations. The average of the measured values of the manufacturing parameters were used in the calculations. The calculation results based on the manufacturing parameters are also shown in table 2.3.

Table 2.3
Calculation for pipe "C" at 5,000 psi

p_c (psi)	σ_o (ksi)	σ_e (ksi)	T_{net} (ft-lb)	ε_z (%)	ε_Θ (%)	TEST PARA.
345.6	113.4	35.1	0	-0.09	3.76	UAD
324.6	100.5	32.8	0	-0.005	3.29	UAM
367.2	112.9	37.3	0	0	3.71	RAD
325.9	100.4	31.2	0	0	3.40	RAM

Expected test results for restrained ends and unrestrained ends were calculated based on pipe as design and as manufactured.
UAD = Unrestrained ends as design
UAM = Unrestrained ends as manufactured
RAD = Restrained ends as design
RAM = Restrained ends as manufactured

2.5 Calculations for pipe "C" (including the liner behaviour) at 5,000 psi

Table 2.4 summarizes the calculations for of pipe "C" at 5,000 psi internal pressure, including the behaviour of the liner as a structural layer. The physical parameters of pipe "C" given in table 2.1 (as designed) were used in the calculations.

The following summarizes the material properties of the structural layers and the liner. The tensile modulus of the structural strips is 3.5×10^6 psi, the Young's modulus of the liner is 145,000 psi. The Poisson's ratio of the liner material is 0.36. The nominal radius r of the pipe, which is one and a half inch, was used in the calculations. In the case of unrestrained end, equations 2.52 and 2.53 were used to calculate the contact pressure between the liner and the hoop layers p_{cp} and the contact between the hoop and the helix layers p_c respectively. In the case of unrestrained ends, equations 2.54 and 2.55 were used to find out the contact pressures, p_{cp} and p_c, respectively. The stresses and strains in the liner and the structural layers are obtained by substituting the values of p_{cp} and p_c into equations 2.42 to 2.51.

Table 2.4
Calculations for pipe "C" (including behaviour of the liner) at 5,000 psi.

p_{cp} (psi)	p_c (psi)	σ_θ (psi)	σ_z (psi)	σ_o (ksi)	σ_e (ksi)	ε_θ (10^{-3})	ε_z (10^{-3})	ε_o (10^{-3})	ε_e (10^{-3})	Cond.
4195.8	326.1	5913.2	2251.0	94.302	33.163	35.2	0.843	26.9	9.475	U.E.
4193.5	308	5930	2134.8	94.687	31.322	35.7	0	27.1	8.949	R.E.

Predicted performance of pipe based on dimensions of the pipe as designed for restrained ends and unrestrained ends
U.E. = Unrestrained ends condition
R.E. = Restrained ends condition

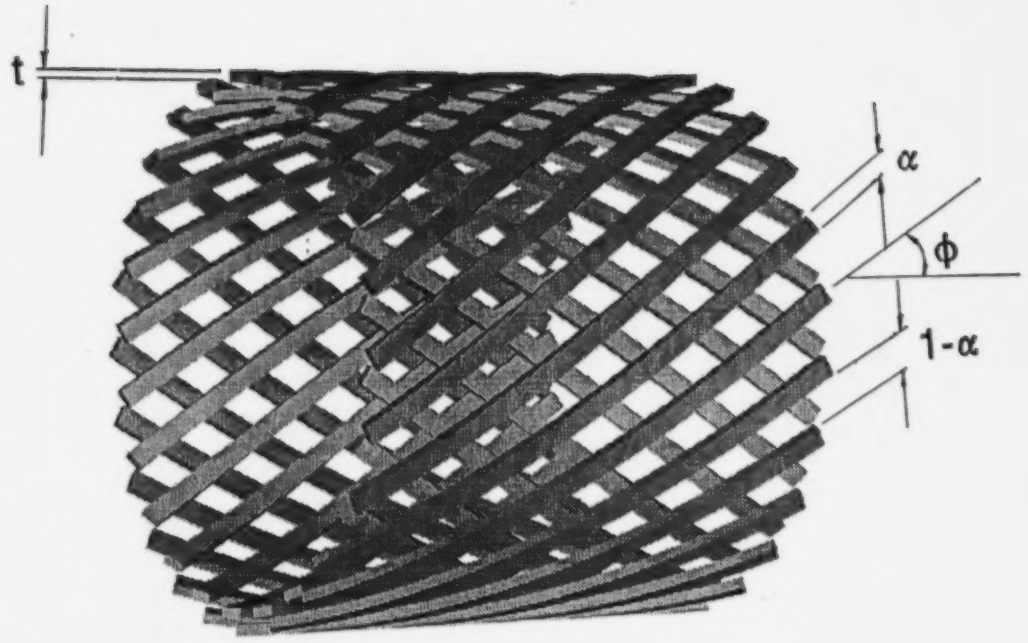

Figure 2.1
Simple model. The liner, which serves as a non-structural barrier to internal pressure is not shown. α is shown as the fraction of composite in a layer for one strip width. t is the radial thickness of a layer.

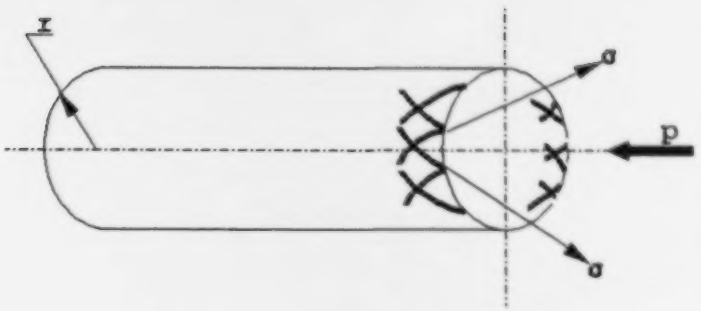

Figure 2.2A
Transverse plane of a simple model, axial loading of the structural layers (Only the ends of some helical strip are shown.).

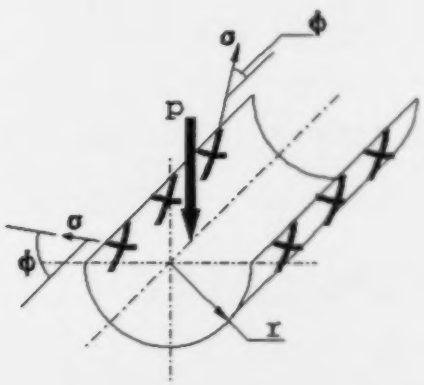

Figure 2.2B
Sectioned diametral plane of half structural layers in a simple model, radial loading (Only the ends of some helical strips are shown.).

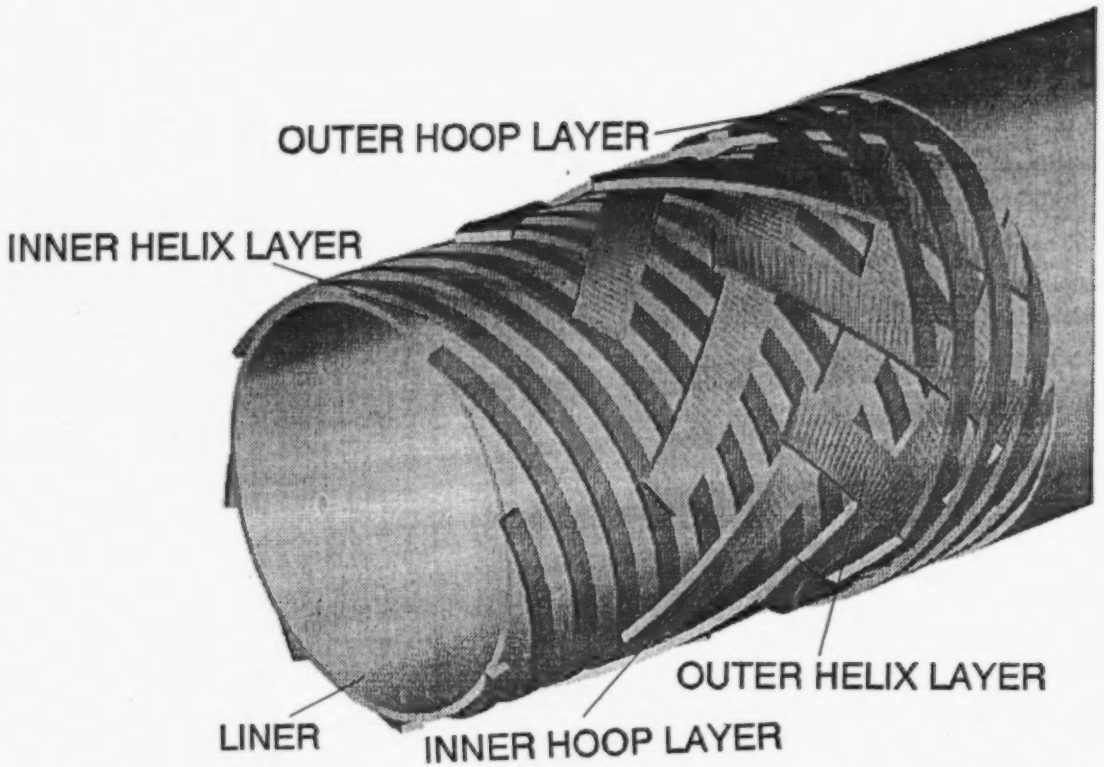

Figure 2.3
Complex model with structural strips and liner only, elastomer strips are not shown.

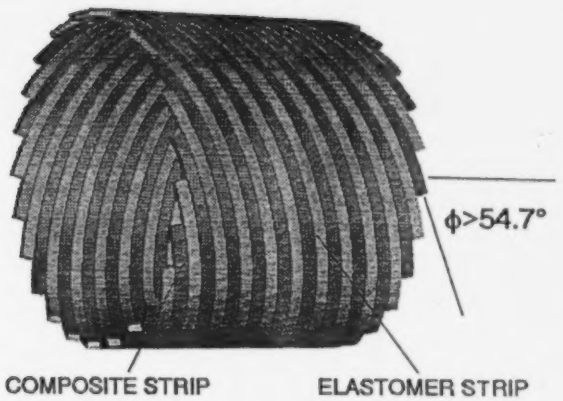

Figure 2.4
Basic hoop layer construction, composite strips are separated by elastomer strips.

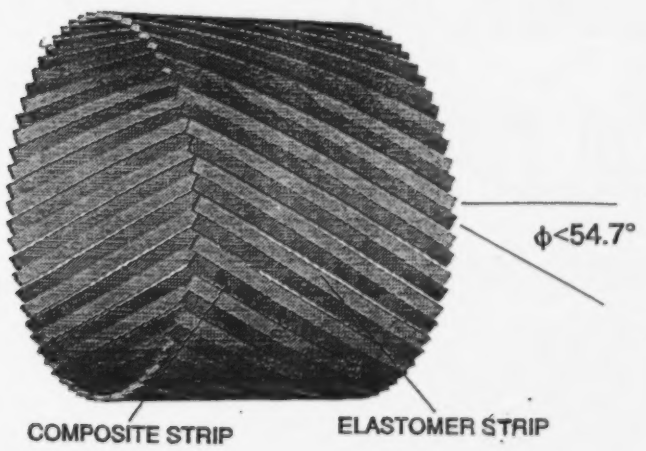

Figure 2.5
Basic helix layer construction, composite strips are separated by elastomer strips.

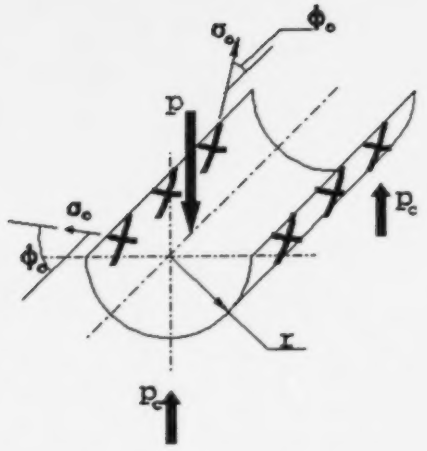

Figure 2.6A
Sectioned diametral plane of half hoop layers in a complex model, radial loading of hoop layers (Only the ends of some strips are shown.).

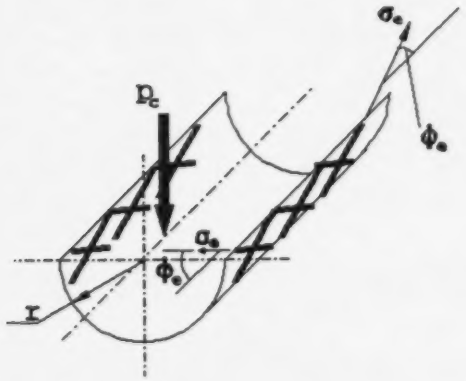

Figure 2.6B
Sectioned diametral plane of half helix layers in a complex model, radial loading of helix layers (Only part of the strips is shown.). Internal pressure p_c is applied by the hoop layers.

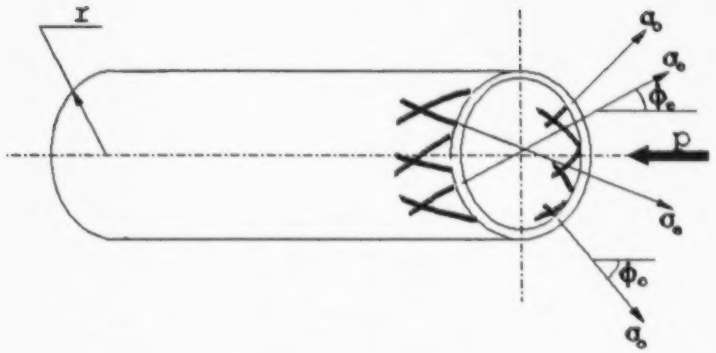

Figure 2.6C
Transverse plane of a complex model, axial loading of the structural layers.

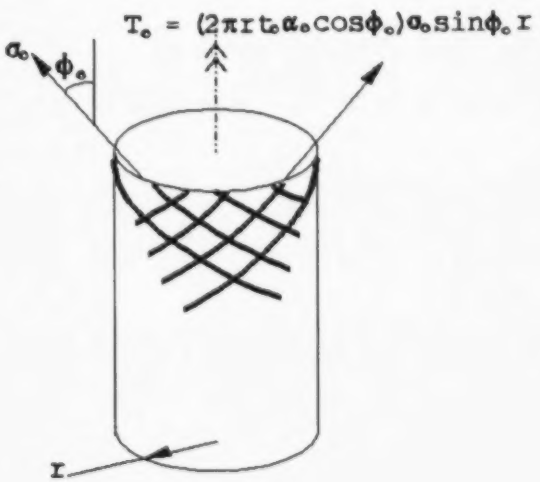

Figure 2.7
Torque generated by a single hoop layer of a complex model. T_o is the torque generated by the hoop layer.

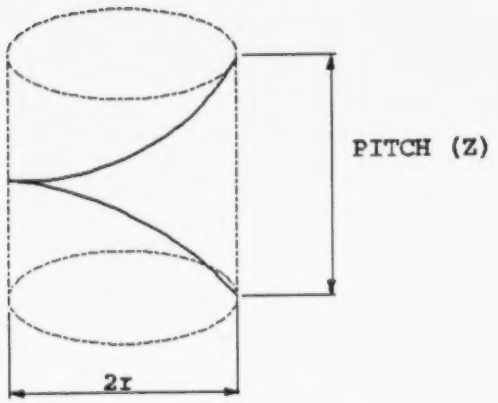

Figure 2.8A
Geometry of one helical pitch.

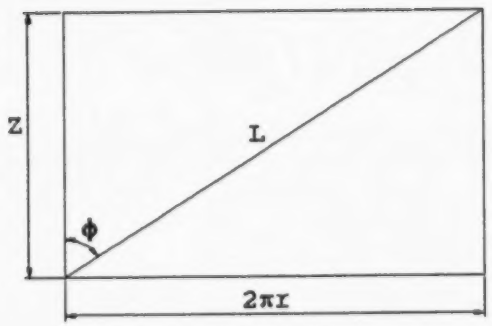

Figure 2.8B
Development view of one pitch of a strip.

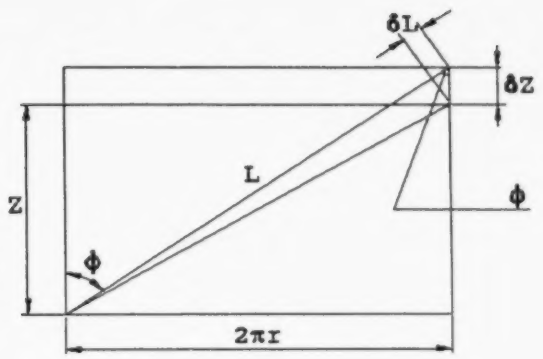

Figure 2.9
Schematic of longitudinal pipe deformation.

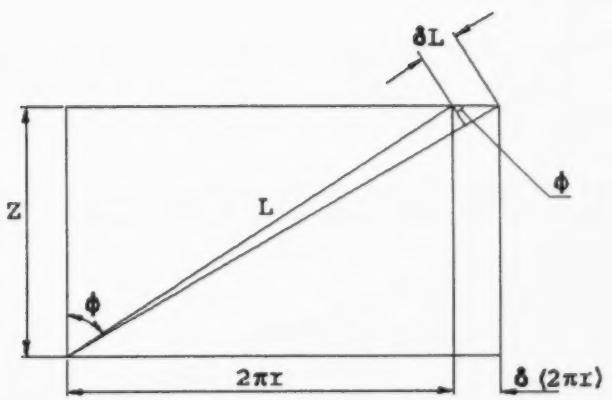

Figure 2.10
Schematic of circumferential pipe deformation.

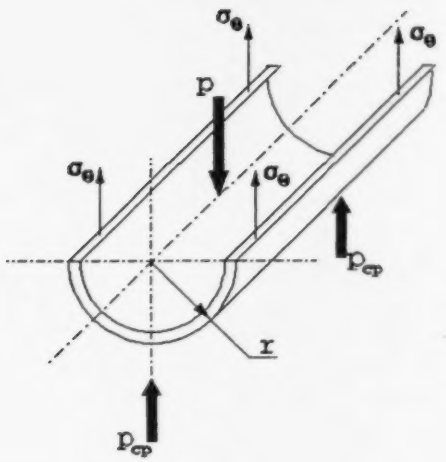

Figure 2.11A
Sectioned diametral plane of a half liner in a simple model, radial loading of the liner. p_{cp} is the contact pressure between the liner and the structural layers.

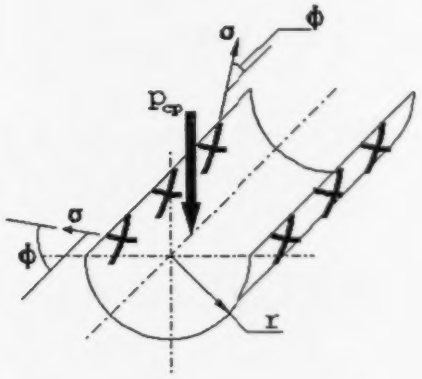

Figure 2.11B
Sectioned diametral plane of half structural layers in a simple model, radial loading of the structural layers. P_{cp} is the internal pressure of the structural layers.

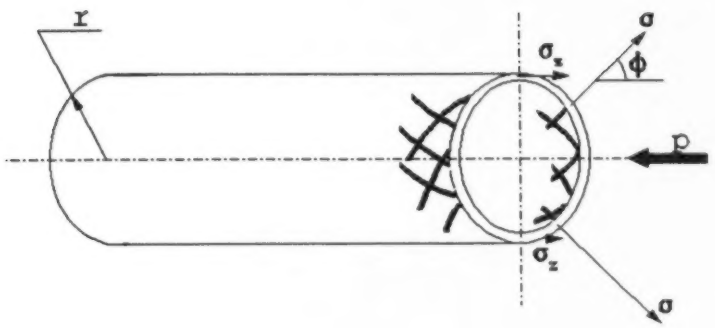

Figure 2.11C
Transverse plane of a simple model (including the liner), axial loading of the liner and the structural layers.

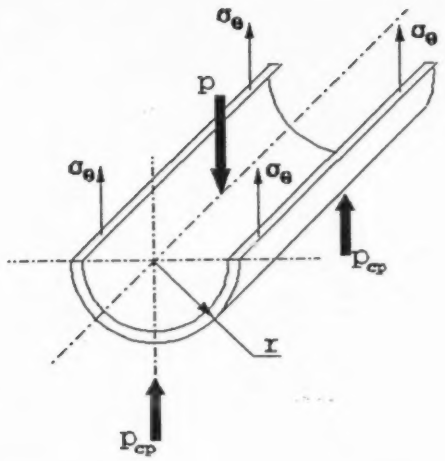

Figure 2.12A
Sectioned diametral plane of a half liner in a complex model, radial loading of the liner. p_{cp} is the contact pressure between the liner and the structural layers.

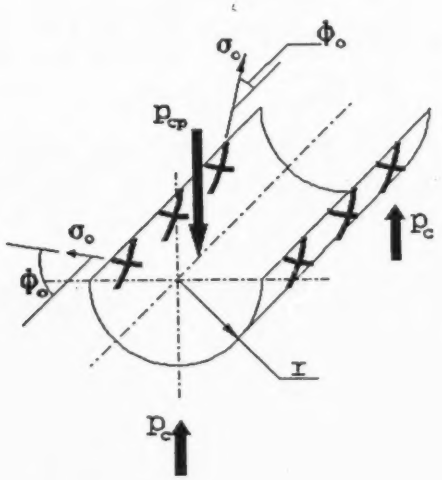

Figure 2.12B
Sectioned diametral plane of half hoop layers in a complex model, radial loading of the hoop layers. p_{cp} is the contact pressure between the liner and the hoop layers, p_c is the pressure acting by the helix layers onto the hoop layers due to internal pressure of the pipe.

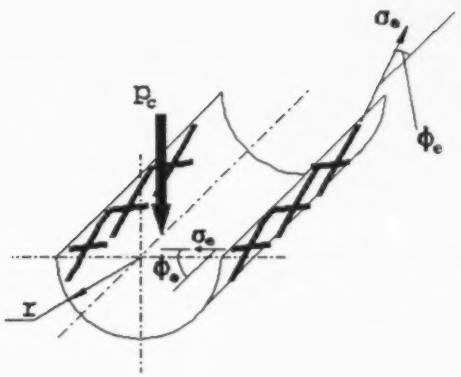

Figure 2.12C
Sectioned diametral plane of half helix layers in a complex model, radial loading of the helix layers. p_c is the contact pressure between the hoop and helix layers.

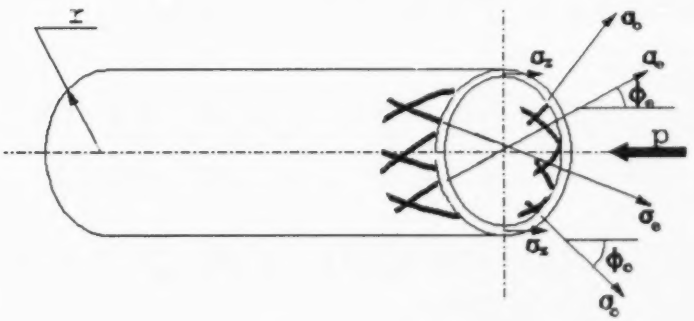

Figure 2.12D
Transerve plane of a complex model, axial loading of the liner and the structural layers.

Chapter 3 Thermal Effect

When transporting a fluid at temperature higher than the temperature during manufacturing, the liner and the structural layers may experience a temperature increase. The materials in each layer have different coefficients of thermal expansion so that the various components of the pipe do not experience uniform circumferential expansion which causes physical interference and thermal stresses. In the following discussion the temperature distribution is taken to be axi-symmetric and constant along the length of the pipe. The deformation of the pipe is assumed to be axi-symmetric. During thermal deformation the cross section is assumed to remain plane, meaning that the unit elongations in the direction of the pipe axis are constant.

The ends of the pipe can be restrained or unrestrained. It is assumed that the structural layers are symmetrically wrapped along the pipe (two hoop layers and two helix layers), and no rotation occurs on the pipe when there is a temperature change. The following analysis predicts the thermal stress generated in the polymer liner and composite strips. The tensile modulus of the elastomer strips is so low that the thermal stress on the elastomer strip is neglected.

3.1 Simple model

The simple model of the pipe consists of two identical structural layers wrapped with opposite hand. In this analysis, it is assumed that initially the liner and structural layers are at the same temperature and no stresses exists. The liner is given a uniform temperature change δT_p and the structural layers are given a uniform temperature change δT_c. It is assumed that no separation occurs between the liner and the structural layers.

When there is temperature change in the liner or the structural layers, a thermal contact pressure between the liner and the structural layers (p_i) will develop. This thermal contact pressure causes compressive hoop stress in the liner. This hoop stress in the liner can be written as

$$\sigma_\theta = \frac{-p_t r}{t_p} \quad , \tag{3.1}$$

where p_t is the contact pressure between the structural layers and the liner due to thermal effect.

The relationship between contact pressure and stress induced in the structural layers was defined in equation 2.33. However, the pressure acting on the structural layers is replaced by the thermal contact pressure (p_t) between the liner and the structural layers and the stress in the structural layers is replaced by the thermal stress (σ_c) in the structural layers in this analysis.

Then

$$\sigma_c = \frac{p_t r}{2 t_c \alpha \sin^2 \phi} \quad . \tag{3.2}$$

The total longitudinal strain of the pipe is equal to the sum of the thermal strain of the liner and the strain resulting from hoop stress and longitudinal stress in the liner.

$$\varepsilon_z = a_p \delta T_p + \frac{\sigma_z}{E_p} - \frac{\mu \sigma_\theta}{E_p} \quad , \tag{3.3}$$

where a_p is the coefficient of linear thermal expansion of the liner material.

Similarly, the total circumferential strain of the pipe is equal to the sum of the thermal strain of the liner and the strain due to the hoop stress and the longitudinal stress in the liner.

Then

$$\varepsilon_\theta = a_p \delta T_p + \frac{\sigma_\theta}{E_p} - \frac{\mu \sigma_z}{E_p} \quad . \tag{3.4}$$

The total strain (ε_c) of the composite strips is equal to the sum of the thermal strain and the strain in the composite strips due to the thermal contact pressure. The thermal contact pressure generates a stress in the composite strips, this stress results in a strain in the composite strips.

Then

$$\varepsilon_c = a_c \delta T_c + \frac{p_i r}{2 t_c \alpha E_c \sin^2\phi} \quad , \tag{3.5}$$

where a_c is the coefficient of linear thermal expansion of the composite material.

The relationship between strain in the pipe and strain in the structural strips expressed in equation 2.19 is also applicable in this analysis, since there is no separation between the structural layers and the liner.

That is

$$\varepsilon_c = \varepsilon_\theta \sin^2\phi + \varepsilon_z \cos^2\phi \quad . \tag{3.6}$$

For axial force equilibrium to exist in the pipe, the resulting force acting along the pipe axis must be equal to the total longitudinal force acting on the polymer layer and the composite strips. In the case where the pipe is free to expand longitudinally, the resultant force at the pipe ends must be equal to zero. Hence

$$F_{re} = 2\pi r t_p \sigma_z + 2 t_c \alpha \cos^2\phi 2\pi r \sigma_c \tag{3.7}$$

or

$$\frac{F_{re}}{2\pi r} = 0 = t_p \sigma_z + 2 t_c \alpha \cos^2\phi \sigma_c \quad . \tag{3.8}$$

Equations 3.3, 3.4 and 3.5 are the strain equations for the polymer liner and the composite strips. Equations 3.1 and 3.2 are the equilibrium equations and equation 3.6 is the compatibility equation. Equation 3.8 expresses the equilibrium condition at the pipe end under free expansion condition.

Restrained Ends

When the pipe is restrained at both ends, the change in temperature will induce thermal stresses. The thermal stress in the liner may cause buckling, however, in this analysis it is assumed that buckling of the pipe does not occur, as would be the case of

a pipe buried underground pipe. In this case, ε_z is zero and so the resultant force acting along the pipe axis is not zero. Equation 3.7 can be used to determine the axial force on the pipe due to temperature change. There are six unknowns and six independent equations. The unknowns are p_i, ε_θ, ε_c, σ_c, σ_z, and σ_θ.

Solving these six simultaneous equations gives

$$p_i = \frac{a_p \delta T_p (1+\mu)\sin^2\phi - a_c \delta T_c}{\frac{r}{2t_c \alpha E_c \sin^2\phi} + \frac{r(1-\mu^2)\sin^2\phi}{E_p t_p}} \quad . \tag{3.9}$$

The circumferential stress in the liner σ_θ, and the stress and strain in the composite strips can be obtained by substituting p_i into equation 3.1, equation 3.2, and equation 3.5 respectively. The longitudinal strain and circumferential strain of the liner can be obtained by solving equation 3.3 and equation 3.4 simultaneously.

Unrestrained ends

In this case, ε_z is not equal to zero; instead, the pipe is free to expand. Thus, buckling will not occur in this condition. The resultant force acting along the pipe axis will be zero because the pipe is free to expand. Equation 3.7 can be applied in this case. Therefore, there are seven unknowns, p_i, ε_θ, ε_c, σ_c, σ_θ, σ_z and ε_z, equations 3.1 to 3.7 are used simultaneously to solve for these unknowns.

After solving these seven simultaneous equations, p_i can be written as

$$p_i = \frac{a_p \delta T_p - a_c \delta T_c}{r\left[\frac{\sin^2\phi - \mu\cos^2\phi}{E_p t_p} + \frac{\cot^2\phi(\cos^2\phi - \mu\sin^2\phi)}{E_p t_p} + \frac{1}{2t_c \alpha E_c \sin^2\phi}\right]} \quad . \tag{3.10}$$

In similar fashion to the condition of restrained ends, the other unknowns can be obtained after p_i is found. It is also shown from equations 3.9 and 3.10 that p_i becomes zero when E_p of the liner is very low or when the liner experiences load relaxation.

3.2 Complex model

The effect of temperature in the complex model is similar to that of the simple model. The thermal contact pressure p_α between hoop layers and helix layers is taken into consideration. It is assumed that the coefficients of thermal expansion of the hoop layers and helix layers are the same. In addition, different temperature change in different layers are considered in this discussion, approximating a thermal gradient in the radial direction.

The general equations used in this analysis are similar to the simple model analysis. The hoop stress developed in the polymer liner resulting from the thermal contact pressure when the temperature changes is expressed as

$$\sigma_\theta = -\frac{p_i r}{t_p} \quad . \tag{3.11}$$

Similar to equation 2.4, the total tensile stress induced in the hoop strips due to the thermal contact pressure p_α and the thermal contact pressure p_i is

$$\sigma_o = \frac{(p_i - p_\alpha) r}{2 t_o \alpha_o \sin^2 \phi_o} \quad . \tag{3.12}$$

Similarly, the total tensile stress induced in the helix strips due to the thermal contact pressure between the hoop and helix layers is

$$\sigma_e = \frac{p_\alpha r}{2 t_e \alpha_e \sin^2 \phi_e} \quad . \tag{3.13}$$

As in the simple model analysis, the total strain of the hoop strips due to change in temperature and the tensile stress acting in the strips is

$$\varepsilon_o = a_c \delta T_o + \frac{(p_i - p_\alpha) r}{2 t_o \alpha_o E_o \sin^2 \phi_o} \quad . \tag{3.14}$$

Likewise, the total strain of the helix strips is expressed as

$$\varepsilon_e = a_e \delta T_e + \frac{p_a r}{2 t_e \alpha_e E_e \sin^2 \phi_e} \quad . \tag{3.15}$$

Similar to the simple model analysis, the longitudinal strain of the pipe is expressed as

$$\varepsilon_z = a_p \delta T_p + \frac{\sigma_z}{E_p} - \frac{\mu \sigma_\theta}{E_p} \quad . \tag{3.16}$$

Once again, the circumferential strain in the pipe resulting from the change in temperature, and the hoop stress and longitudinal stress in the liner is

$$\varepsilon_\theta = a_p \delta T_p + \frac{\sigma_\theta}{E_p} - \frac{\mu \sigma_z}{E_p} \quad . \tag{3.17}$$

The relationship between the pipe strains and the strains of the hoop and helix layers has been related in equations 2.22 and 2.23, which can be applied in this analysis,

$$\varepsilon_o = \varepsilon_\theta \sin^2 \phi_o + \varepsilon_z \cos^2 \phi_o \quad , \tag{3.18}$$

and

$$\varepsilon_e = \varepsilon_\theta \sin^2 \phi_e + \varepsilon_z \cos^2 \phi_e \quad . \tag{3.19}$$

A resultant force acting along the pipe axis at the pipe end resulting from the stresses in the liner, hoop layer and helix layer develops. Their relationship is expressed as

$$F_{re} = 2\pi r t_p \sigma_z + 4\pi r t_o \alpha_o \cos^2 \phi_o \sigma_o + 4\pi r t_e \alpha_e \cos^2 \phi_e \sigma_e \quad .$$

In the case of zero net axial force on the structure, this axial force equation reduces to

$$\frac{F_{re}}{2\pi r} = 0 = t_p \sigma_z + 2 t_o \alpha_o \cos^2 \phi_o \sigma_o + 2 t_e \alpha_e \cos^2 \phi_e \sigma_e \quad . \tag{3.20}$$

From the above equations, all the unknowns can be expressed in term of thermal

contact pressure between the liner and the hoop layers (p_t) and the thermal contact pressure between the hoop layers and the helix layers (p_{ct}). Similar to the simple model analysis, once these two parameters have been found, the expressions of the other unknowns can be obtained by substituting p_t and p_{ct} into the respective equations in this section.

Restrained ends

In this case, a restrained end condition, the total axial strain ε_z is equal to zero. The resultant force acting at the pipe ends is not equal to zero. Therefore, Equation 3.20 cannot apply to this condition. This results in nine unknowns, p_t, σ_θ, σ_z, p_{ct}, σ_o, σ_e, ε_o, ε_e and ε_θ. These unknowns can be found by solving equations 3.11 to 3.19 simultaneously. The results of solving these equations are

$$p_{ct} = \frac{a_p \delta T_p (1+\mu)\,[X\sin^2\phi_e - \sin^2\phi_o] + a_c[\,\delta T_o - \delta T_e X]}{r\left[U + \frac{UW}{V} + \frac{TW}{V}\right]} \,, \tag{3.21}$$

and

$$p_t = \frac{a_p \delta T_p (1+\mu)\sin^2\phi_e}{rV} - \frac{a_c \delta T_e}{rV} +$$

$$\frac{W[a_p \delta T_p (1+\mu)\,(\sin^2\phi_o - X\sin^2\phi_e) - a_c(\delta T_o - \delta T_e X)]}{r[UV+UW+TW]} \,, \tag{3.22}$$

where

$$T = \frac{(1-\mu^2)\sin^2\phi_o}{E_p t_p} \,,$$

$$U = \frac{1}{2t_o \alpha_o E_o \sin^2\phi_o} \,,$$

$$V = \frac{(1-\mu^2)\sin^2\phi_e}{E_p t_p} ,$$

$$W = \frac{1}{2t_e\alpha_e E_e \sin^2\phi_e} ,$$

and

$$X = \frac{U+T}{V} .$$

Unrestrained ends

In a free end condition, the pipe is free to expand longitudinally due to temperature changes. The resultant force at the pipe end is equal to zero. Therefore, equation 3.20 has to be taken into consideration. There are then ten unknowns, p_t, σ_θ, σ_z, p_{ct}, σ_o, σ_e, ε_o, ε_e, ε_θ, and ε_z. Solving the ten equations simultaneously, it gives

$$p_t = \frac{a_p\delta T_p(1-\frac{N+Y}{K-J}) - a_c[\delta T_e - \delta T_o\frac{N+Y}{K-J}]}{r[M-\frac{(H+J)(N+Y)}{K-J}]} \qquad (3.23)$$

and

$$p_{ct} = \frac{a_p\delta T_p - a_c\delta T_o}{r[K-J]} - \frac{[a_p\delta T_p(1-\frac{N+Y}{K-J}) - a_c(\delta T_e - \delta T_o\frac{N+Y}{K-J})](H+J)}{r[K-J][M-\frac{(H+J)(N+Y)}{(K-J)}]} \qquad (3.24)$$

where

$$H = \frac{\cot^2\phi_o(\cos^2\phi_o - \mu\sin^2\phi_o) + \sin^2\phi_o - \mu\cos^2\phi_o}{E_p t_p} ,$$

$$J = \frac{1}{2t_o\alpha_o E_o \sin^2\phi_o} ,$$

$$K = \frac{(\cot^2\phi_e - \cot^2\phi_o)(\cos^2\phi_o - \mu\sin^2\phi_o)}{E_p t_p} ,$$

$$M = \frac{\cot^2\phi_o}{E_p t_p}(\cos^2\phi_e - \mu\sin^2\phi_e) + \frac{\sin^2\phi_e - \mu\cos^2\phi_e}{E_p t_p} ,$$

$$N = \frac{1}{2t_e\alpha_e E_e \sin^2\phi_e} ,$$

and

$$Y = \frac{(\cot^2\phi_e - \cot^2\phi_o)(\cos^2\phi_e - \mu\sin^2\phi_e)}{E_p t_p} .$$

3.3 Thermal stresses of an actual pipe

The contact pressures between the liner and the structural layers, p_{ct} and p_t, can be obtained from expressions developed in section 3.2. Thermal stresses and strains developed in a pipe of both restrained and unrestrained ends conditions can be calculated by substituting p_{ct} and p_t into the general equations in section 3.2.

In some applications, the liner and all the structural layers can stabilize at a uniform final temperature. The thermal stresses and strains developed in pipe "C" a common temperature increase in the liner and the structural layers were calculated for both restrained and unrestrained ends conditions. The following describes the calculation parameters for the thermal stress calculation of pipe "C". The temperature increase in the liner, the hoop and the helix layers were assumed to be common at 130°F. The coefficients of linear thermal expansion of the liner and the structural layers were assumed to be 45 x 10^{-6}/°F and 4.5 x 10^{-6}/°F respectively. The tensile modulus of both hoop and helix strips is 3.5 x 10^6 psi. The Young's modulus of the liner material is 145,000 psi and its Poisson's ratio is 0.36. The physical measurements of the pipe "C" were given in table 2.1. Nominal radius of the pipe, which is one and a half inch, is used in the thermal stress calculation. The results of the calculations are shown in table 3.1. The parameters described in this paragraph are also used to calculate the thermal stresses and strains induced in the structural layers when the liner exhibits load relaxation. The calculation results when the liner exhibits load relaxation are shown in table 3.2. When there is a common temperature increase in the liner and each structural layer. Under restrained ends condition, equations 3.21 and 3.22 become

$$p_{ct} = \frac{\delta T[a_p(1+\mu)[I\sin^2\phi_e - \sin^2\phi_o] + a_c[1-I]}{r[\Delta + \frac{\Delta\Xi}{\Lambda} + \frac{\Gamma\Xi}{\Lambda}]}, \qquad (3.25)$$

and

$$p_t = \delta T \left[\frac{a_p(1+\mu)\sin^2\phi_e - a_c}{r\Lambda} + \frac{a_p(1+\mu)(\sin^2\phi_o - I\sin^2\phi_e) - a_c(1-I)}{\frac{r}{\Xi}[\Delta\Lambda + \Delta\Xi + \Gamma\Xi]} \right]. \qquad (3.26)$$

Similarly, under unrestrained ends condition, equations 3.23 and 3.24 become

$$p_t = \delta T \left[\frac{a_p(1-\frac{\Xi+\Omega}{\Pi-\Delta}) - a_c(1-\frac{\Xi+\Omega}{\Pi-\Delta})}{r[\Psi-\frac{(\Sigma+\Delta)(\Xi+\Omega)}{\Pi-\Delta}} \right] \tag{3.27}$$

and

$$p_{ct} = \delta T \left[\frac{a_p-a_c}{r[\Pi-\Delta]} - \frac{a_p(1-\frac{\Xi+\Omega}{\Pi-\Delta}) - a_c(1-\frac{\Xi+\Omega}{\Pi-\Delta})(\Sigma+\Delta)}{r[\Pi-\Delta][\Psi-\frac{(\Sigma+\Delta)(\Xi+\Omega)}{(\Pi-\Delta)}]} \right] . \tag{3.28}$$

When the liner exhibits load relaxation, the expression of p_{ct} under restrained ends condition become

$$p_{ct} = \delta T \frac{a_c(1-\frac{\sin^2\phi_o}{\sin^2\phi_e})}{r(\Delta+\Xi\frac{\sin^2\phi_o}{\sin^2\phi_e})} , \tag{3.29}$$

where

$$\Gamma = \frac{(1-\mu^2)\sin^2\phi_o}{E_p t_p} ,$$

$$\Delta = \frac{1}{2t_o\alpha_o E_o \sin^2\phi_o} ,$$

$$\Lambda = \frac{(1-\mu^2)\sin^2\phi_e}{E_p t_p} ,$$

$$\Xi = \frac{1}{2t_e\alpha_e E_e \sin^2\phi_e} ,$$

$$I = \frac{\Delta+\Gamma}{\Lambda} ,$$

$$\Sigma = \frac{\cot^2\phi_o(\cos^2\phi_o-\mu\sin^2\phi_o)+\sin^2\phi_o-\mu\cos^2\phi_o}{E_p t_p} ,$$

$$\Pi = \frac{(\cot^2\phi_e-\cot^2\phi_o)(\cos^2\phi_o-\mu\sin^2\phi_o)}{E_p t_p} ,$$

$$\Psi = \frac{\cot^2\phi_o}{E_p t_p}(\cos^2\phi_e-\mu\sin^2\phi_e)+\frac{\sin^2\phi_e-\mu\cos^2\phi_e}{E_p t_p} ,$$

and

$$\Omega = \frac{(\cot^2\phi_e-\cot^2\phi_o)(\cos^2\phi_e-\mu\sin^2\phi_e)}{E_p t_p} .$$

Equations 3.25 to 3.28 are used to calculate p_t and p_{ct} under the condition of common temperature increase in the liner and the structural layers. Once, p_t and p_{ct} are found, the stresses and strains in the liner and structural layers can be obtained by substituting p_t and p_{ct} into the general equations in section 3.2. However, p_t in both restrained end and unrestrained end conditions, and p_{ct} in unrestrained ends condition are zero when the liner exhibits load relaxation. Table 3.2 shows the results of calculations when the Young's modulus of the liner become zero. The calculation parameters mentioned above are also used in to the calculation when the liner exhibits load relaxation. Equations 3.16 and 3.17, which are the expressions of longitudinal and circumferential pipe strain, are not applicable when E_p is very small, which is the case when the liner undergoes load relaxation.

For restrained end, comparing the first rows from table 3.1 and 3.2, it is evident that the contact pressure between the liner and hoop layers (p_t) reduces to zero as the liner experiences load relaxation. At the same time, the contact pressure between the hoop and helix layers (p_{ct}) increases, from negative 2.61 psi to negative 12.48 psi, recalling that a negative contact pressure is really not possible, unless superimposed with the load from internal pressure. During loading relaxation, the hoop layers and helix

layers both experience reduced tensile stress.

Making a similar comparison for unrestrained ends by comparing the bottom rows from table 3.1 and 3.2, the load relaxation in the hoop and helix structures is even more pronounced. The stresses in the hoop and helix layers due to temperature change reduce to zero. The axial strain of the pipe and circumferential strain are determined directly from thermal expansion.

Table 3.1
Calculations for pipe "C" when temperature increases in the liner and the structural layers are common at 130°F.

p_t (psi)	p_{ct} (psi)	σ_θ (psi)	σ_z (psi)	σ_o (psi)	σ_e (psi)	ε_θ (10^{-3})	ε_z (10^{-3})	ε_o (10^{-3})	ε_e (10^{-3})	Condition
134.4	-2.61	-987.9	-1203.9	3337.7	-265.5	2.025	0	1.539	0.509	R.E.
139.2	33.40	-1023.5	-974.6	2578.4	3396.0	1.975	1.670	1.321	1.555	U.E.

Calculations include both restrained ends (R.E.) and unrestrained ends (U.E.) conditions.

Table 3.2
Calculations for pipe "C" when the temperature increases in the liner and the structural layers are common at 130°F after the liner undergoes load relaxation.

p_t (psi)	p_{ct} (psi)	σ_o (psi)	σ_e (psi)	ε_θ (10^{-3})	ε_z (10^{-3})	ε_o (10^{-3})	ε_e (10^{-3})	Condition
0	-12.48	304.3	-1269.6	0.884	0	0.672	0.222	R.E.
0	0	0	0	0.585	0.585	0.585	0.585	U.E.

Calculations include both restrained ends (R.E.) and unrestrained ends (U.E.) conditions.

Chapter 4 End Connection

The end connection design and the mechanisms, which allow it to perform its function are discussed in this chapter. The assembly procedures of the end connection to the prototype are also described in this chapter.

4.1 End connection design

The end connection is used to connect the pipe to other equipment or pipe through a standard flange. The connection was designed to connect with existing steel flange components presently used in the steel piping industry. A detailed sketch of the end connection assembly is shown in Figure 4.1. Veritec Offshore Technology and Services [6] suggest that the interface between flexible pipe and the end fitting should have at least the same structural integrity as the flexible pipe itself. This becomes the objective in the end connection design discussed in this chapter. The end connection is designed and tested to ensure that it equals or exceeds the maximum axial load in the pipe due to transportation and service loading. The axial load can result from external axial tension or can be generated by internal pressure.

The end connection is an assembly that mechanically terminates each of the structural layers of the pipe. The end connection includes three major steel components, the cup , the cone and the threaded flange. The flange end of the cone was threaded onto the threaded flange. The threaded flange was modified from a standard ANSI flange. A high density polyethylene stub end which has the same radial dimensions as the liner was inserted through the threaded flange. The threaded flange provides a sliding fit for the stub end to slide through. The trimmed end of the stub end was exposed through the threaded flange, this exposed end was fused to the liner. The liner protruded approximately one half inch from the inner hoop layer and was fused to a stub end. Alignment between the stub end and the liner was set carefully while the pipe was in the fusion machine.

The flange of the fused stub end was compressed by the threaded flange and the connection flange of the connecting equipment by tightening the nuts on the stud bolts.

The flange of the stub end was used as a gasket to seal off any leakage at the connection. Therefore, a high tightening torque was required on the nuts tightening the threaded flange. A steel compression set ring was used to prevent extrusion of stub end flange under high internal pressure. The cup compressed the structural strips against the cone to hold the strips in position when the pipe was under load. The nuts "C" (see figure 4.1) securing the cup were less tight relative to those on the threaded flange since the nuts "A" and "B" were used to compress the flange of the stub end as a gasket to carry the testing pressure. Therefore, the tightening torque on the these nuts must be very high (it was estimated to be 1,500 ft-lb). On the other hand, the nuts "C" were only used to hold the structural strips and the cup in position. Hence, the tightening torque required was much lower (it was estimated to be 100 ft-lb).

The inner and outer helix strips were wrapped on the outside surface of the cone. The position at which the structural layers separated from the pipe is defined as the take off point. The last six inches of the structural strips from the flange end were braided together. This braided structure provides anchorage which prevented sliding movement between the two helix layers inside the cup and cone assembly and the helix layers relative to the cup and cone when the pipe was under axial load. A shoulder was machined in both cup and cone to allow steel cables to be triaxially braided in the area of the shoulder.

These braided steel cables prevent interlaminar shear on the helix layers so that the structural integrity preventing pull out of the braided helix layers. The braided steel cables also served as a fastening mechanism for the braided helix layer. In order to hold the outer hoop layer inside the end connection assembly, the outer hoop strips were also braided together with the helix strips at the last six inches from the flange end of the cone.

The cup was designed to provide uniform contact pressure at the cross over points of the braided structural strips. The same cone angle was used on both the cup and cone. When the cup was tightened against the threaded flange, the cross over points of the strips were compressed by the internal surface of the cup. Pre-tensioning on the pipe was then performed in order to remove any slack on the braided structure. It is believed

that a better load distribution in the structural strips was achieved after any slack was eliminated by pre-tensioning. The space between the internal surface of the cup and the external surface of the cone was then filled by injected polyurethane. The average hardness of the cured polyurethane is 70 Shore D. The injected material inside the cup fills all the spaces of the removed elastomer strips in the outer hoop layer and helix layers inside the cup and cone assembly. After the injected polyurethane was cured, the structure was referred to as a braided injected structure (BIS).

In detail, the end connection assembly procedure was carried out as follows:

1. The flexible composite pipe was cut to an overall length of nineteen and a half feet.
2. The cup was placed over the pipe (pipe end of the cup first) at a distance of twenty one inches from the pipe end so that there was enough space for the subsequent steps.
3. A hose clamp was tightened on to the pipe twenty inches from the end.
4. The outer hoop elastomer strips were cut to nineteen and a half inches from the end of the pipe.
5. The outer hoop composite strips were peeled back from the pipe end all the way to the hose clamp.
6. The exposed layer of polyethylene film was removed up to the hose clamp.
7. The outer helix elastomer strips were cut to nineteen and a half inches from the end of the pipe.
8. The outer helix composite strips were peeled back from the pipe end all the way to the hose clamp.
9. The exposed layer of polyethylene film was removed all the way to the hose clamp.
10. The inner helix elastomer strips were cut to nineteen and a half inches from the end of the pipe.
11. The inner helix composite strips were peeled back from the pipe end all the way to the hose clamp.
12. The exposed layer of polyethylene film was removed all the way to the hose

clamp.

13. The cone (pipe end of cone) was placed at the pipe end as close as possible to the hose clamp.
14. Three inches of the inner hoop layer and the liner was removed from each end.
15. A hose clamp was placed over the inner hoop layer one inch from the end of the pipe and tightened.
16. A half inch of the inner hoop layer was removed to expose the liner for fusion.
17. The stub end was inserted through the threaded flange, and trimmed so that it extended two and a quarter inches beyond the threaded flange. The threaded flange was positioned at the end of the pipe.
18. While the stub end was being supported and the pipe was also being supported (at the exposed inner hoop layer), the stub end was fused to the exposed liner.
19. The flashing was removed from the liner joint.
20. The cone was moved to the threaded flange and screwed on.
21. The inner and outer helix layers were wrapped on the cone. Once this was done, the last six inches at the flange end of the cone was braided.
22. The outer hoop layer was wrapped as tight as possible on the helix layers.
23. A one eighth inch steel wire was braided together with the helix and the hoop layers to a length of one inch from the shoulder of the cone.
24. A quarter inch steel wire was braided together with the helix and the hoop layers to a length of one inch from the previous braided steel wire.
25. The steel compression set ring was placed on the blind flange.
26. The cup was moved over onto the braided cone.
27. The cup was tightened to the threaded flange, assuring the injection inlet hole is at the bottom of the cup.
28. The blind flange and the threaded flange was tightened together against the compression set steel ring by tightening the nuts on the stud bolts.

29. The pipe was pre-tensioned to 1,000 lb axial load.
30. A sheet metal conical dam was constructed at the pipe end of the cup to allow polyurethane to fill the space between the sheet metal and the outer hoop layers.
31. A silicone dam was constructed at the flange of the cup. The silicone was allowed to cure, excessive silicone was removed.
32. Seventy five cubic inches of polyurethane were mixed with seventy five cubic inches of hardener.
33. The mixed polyurethane was injected into the void between the cup and the cone and the space between the cone and the liner simultaneously.
34. Two heat lamps were placed at the end connection area to help curing. The curing time was about six hours at 150°F.
35. The sheet metal dam was removed.
36. The pipe was mounted on to the testing facility.
37. Two equally spaced supports were used to support the pipe.

4.2 End connection mechanisms

Reference [7] states that there are three major mechanisms for the end connection to carry the tensile load of the pipe which will be generated by internal pressure. These are as follows:

1. Bonding mechanism

   The injected polyurethane inside the cup provides an adhesive bonding to the cup, the cone and the structural strips. This adhesive bonding holds the cup, cone and the structural strips together to resist the tensile load of the pipe. It also adheres the structural strips together to form the BIS.

2. Volume mechanism

   The volume mechanism describes the phenomenon of pulling the BIS through an annulus of progressively smaller diameter. This "pulling through" is prevented by the incompressibility of the BIS. The volume mechanism provides a positive anchorage to the BIS. This mechanism was observed by analyzing the stress distribution on the cup and cone from the results of end connection tensile tests. The contact pressure between the BIS and the surfaces on the cup and cone will increase due to more compression on the BIS during the "pulling through". This was also verified by the results of end connection tensile tests.

3. Band brake

   When the pipe is under axial tension, the band brake mechanism on the BIS transfers the axial load to the cone through the friction between the BIS and the external surface of the cone, and internal surface of the cup. The contact pressure between the BIS and the external surface of the cone increases with the increase of axial load. This increase in contact pressure increases the frictional force between the BIS and the external surface of the cone. The band brake mechanism was observed by the stress analysis on the cone [7]. However, the band brake mechanism requires an anchor of one end of the BIS, this anchorage is provided by the injected material behind the shoulders of both cup and cone. In addition, the braided steel cable in between the cup and the cone provides the anchorage of the BIS.

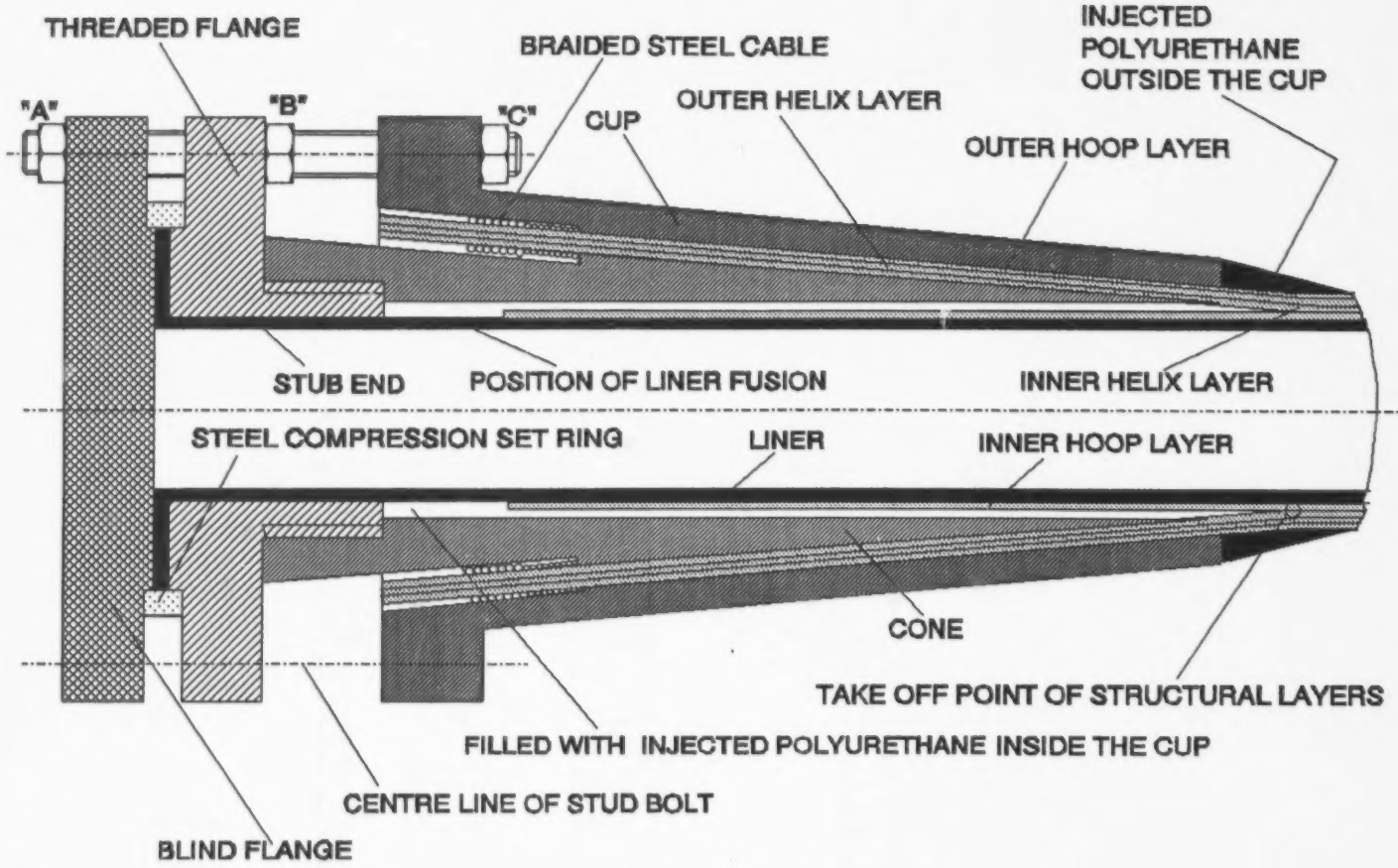

Figure 4.1
End connection assembly of pipe "C"

Chapter 5 Testing Facilities and Testing Procedures

For pipe "C", tests were prepared to verify its pressure capacity and the characteristic of zero strain and rotation when under internal pressure. A cyclic pressure test was also planned. Not all tests were completed because of specimen failure early in the test program. In the static pressure test, pipe rotation at one end (rotating end), axial and transverse displacement at the other end (non-rotating end), and diameter at the middle of the pipe were measured in pressurization steps. The second part of the static pressure test was conducted with restrained ends. This was not conducted due to prior failure. A load cell for measuring torque and axial load was developed for the restrained ends test. The cyclic pressure test was planned for five thousand cycles of 0 - 2,500 psi, but this test was not conducted. Measurement of strain in the structural strips using strain gages was planned but not conducted. Special testing facilities were required in order to carry out these tests. These are described in this chapter. The following discussion summarizes the design of some major testing equipment for the tests.

5.1 Testing facilities

Load cell

A load cell was designed to measure the torque and axial load in the pipe of restrained ends condition. The load cell is capable of measuring the torque generated by the internal pressure or an external torque applied to the pipe. At the same time, the load cell can also measure the axial load generated on the pipe during hydrostatic test and tensile stiffness test. Figure 5.1 shows the arrangement of the strain gages on the load cell.

For a balanced pipe, the net torque generated should be zero. However, the torque generated by adjacent structural layers may not be completely balanced for various reasons, such as manufacturing error or behaviour of the specimen different from the theoretical model. Hence, net torque may be generated by internal pressure. It is also anticipated that torsional test will be required to measure the torsional stiffness of the composite pipe.

Axial load was to be measured in a restrained end pressure test. If a restrained end pipe is designed to have a negative strain when it is under internal pressure, axial tension would occur under internal pressure.

The bridge circuit used in both torque and axial load measurement is a four arm Wheatstone bridge with a constant DC voltage supply. Electrical resistance strain gages are used in the circuit. The torque is measured by a set of strain gages arranged at the angles of $\pm 45°$. And the axial load is measured by the other set of strain gages installed at $0°$ or $90°$. The circuit can provide temperature and bending compensation effects.

Cyclic test control device

Five thousand cycles of 0 - 2,500 psi were required to fulfil the objective of the cyclic pressure test. The cyclic test was regarded as part of the initial test in reference [8] to find out the long-term hydrostatic strength of the pipe. An automatic control system was developed to operate a solenoid spool valve to achieve this purpose. Figure 5.2 shows the schematic of the electronic circuit of the control mechanism. The following discussion describes the working mechanism of the control device.

A pressure transducer is used to monitor the internal pressure in the pipe and send a signal to the electronic control device. This signal is fed to a pair of comparators, where the control points are detected. When the upper (high pressure) control point is detected, a delay is initiated. After the time delay, the output flip-flop changes state to de-energize the solenoid valve. Then the pressure inside the test pipe drops, and when the lower (low pressure) control point is reached, another delay is initiated, after which the output flip-flop changes state to energize the solenoid valve. The electro-mechanical counter is energized for counting during the energizing of the solenoid valve. This cycle continues until the control device is switched off manually. The time delays inside the control mechanism are adjustable so that the pressure inside the pipe can be held for a desired length of time.

The solenoid valve is driven by a solid state relay which provides zero voltage switching to eliminate inductive spikes. The inductive spikes may interfere with the rest of the electronic circuit and cause false triggering. The solenoid spool valve provides

a way of either supplying fluid (pressure increase) or draining fluid (pressure decrease). The supply configuration allows the testing fluid coming from the pump through the spool valve to the pipe. The drain configuration allows the testing fluid to drain from the pipe to the receiver through the spool valve. The timing diagram of the control logic is shown in Figure 5.3.

Pressure intensifier

The pressure intensifier was used to supply and maintain a desired testing pressure inside the pipe. The major component of the pressure intensifier was an air operated positive piston pump. The output pressure is proportional to the air pressure supplied to it at a ratio of approximately 100/1. The output pressure limit set point is determined by a back pressure regulator, which regulates the output pressure. When the output pressure becomes higher than the set pressure, the regulator will maintain the desired pressure inside the test pipe. When the fluid pressure at the inlet of the back pressure regulator becomes 10,000 psi, no air flow is allowed to the pressure intensifier. The output pressure of the pressure intensifier is accurate to 200 psi.

5.2 Testing procedure

The target pressure for the hydrostatic testing of pipe "C" was 5,000 psi. Only the measurements of rotation, axial and transverse displacement, and pipe diameter were taken in the proof test. The procedure of the proof test basically followed the procedure of [9], which is applicable for hydrostatic pressure testing of valves, pipes or containers with sealed connecting ends. Figure 5.4 shows the arrangement of the apparatus used in the test. The following paragraphs describe the procedures of the test.

The testing fluid used was a mixture of water soluble oil and water. This specific mixture was required to prevent corrosion of the pressure intensifier. The pipe was filled with the testing fluid by a gear pump, which had a higher flow rate than the pressure intensifier. The testing fluid entered the pipe through a fill/drain valve located at the lowest point of the pipe. When the pipe was filled with testing fluid, the testing fluid supply was switched manually from the gear pump to the pressure intensifier. An isolating valve with 10,000 psi rating was installed between the gear pump and the pressure intensifier in order to protect the gear pump. Air trapped inside the pipe was vented in order to build up the testing pressure and minimize the stored energy. The vent valve rated at 10,000 psi was located at the highest point of the pipe.

Both unrestrained and restrained tests were planned with the unrestrained test to be done first. In the unrestrained test, the pipe was free to rotate at one end (rotating end). Also, the pipe was allowed to extend and move freely horizontally at the other end (non-rotating end). Pipe rotation was measured at the rotating end. Pipe rotation was obtained by releasing the clamping bolts of a pinch block. The pinch block was used to clamp the pipe in order to measure the torque generated on the pipe resulting from internal pressure. The pipe rotation was measured by the circumferential translation of the torque actuation wheel in inches. The angle of rotation in radian was then obtained by dividing the measured reading by the radius of the wheel. Figure 5.5 and Figure 5.6 show the pictures of rotating end and non-rotating end respectively.

The non-rotating end was supported on a low friction unrestrained test jig, on which the pipe end was free to move horizontally. A reference grid was drawn on the floor for movement measurement. In addition, the diameter at the middle of the pipe was

measured by using a OD measuring tape. The testing pressure was recorded from a pressure gage mounted on the pressure intensifier. The pressure gage provided an appropriate reading on the output of the pressure intensifier. A more accurate reading was obtained from a calibrated pressure transducer, which was mounted on a tee connected to the highest position of the flange at the non-rotating end. The signal from the pressure transducer was connected to a multimeter, whose voltage reading provided the internal pressure measurement.

The pressure inside the pipe was developed gradually by the pressure intensifier. The first holding pressure was 1,000 psi. The holding period for each holding pressure was ten minutes. All the measurements were taken during the pressure holding period. After each holding time, the pressure was released gradually to zero psi and held for ten minutes to allow the pipe to recover. After ten minutes of the recovery period, the pressure was built up gradually again. The pressure held at the next cycle was 1,000 psi higher than the last holding pressure. This pressurization and de-pressurization process was planned to continue until 5,000 psi internal pressure was achieved. After 5,000 psi internal pressure, the pressure inside the pipe would be released and the test would be complete.

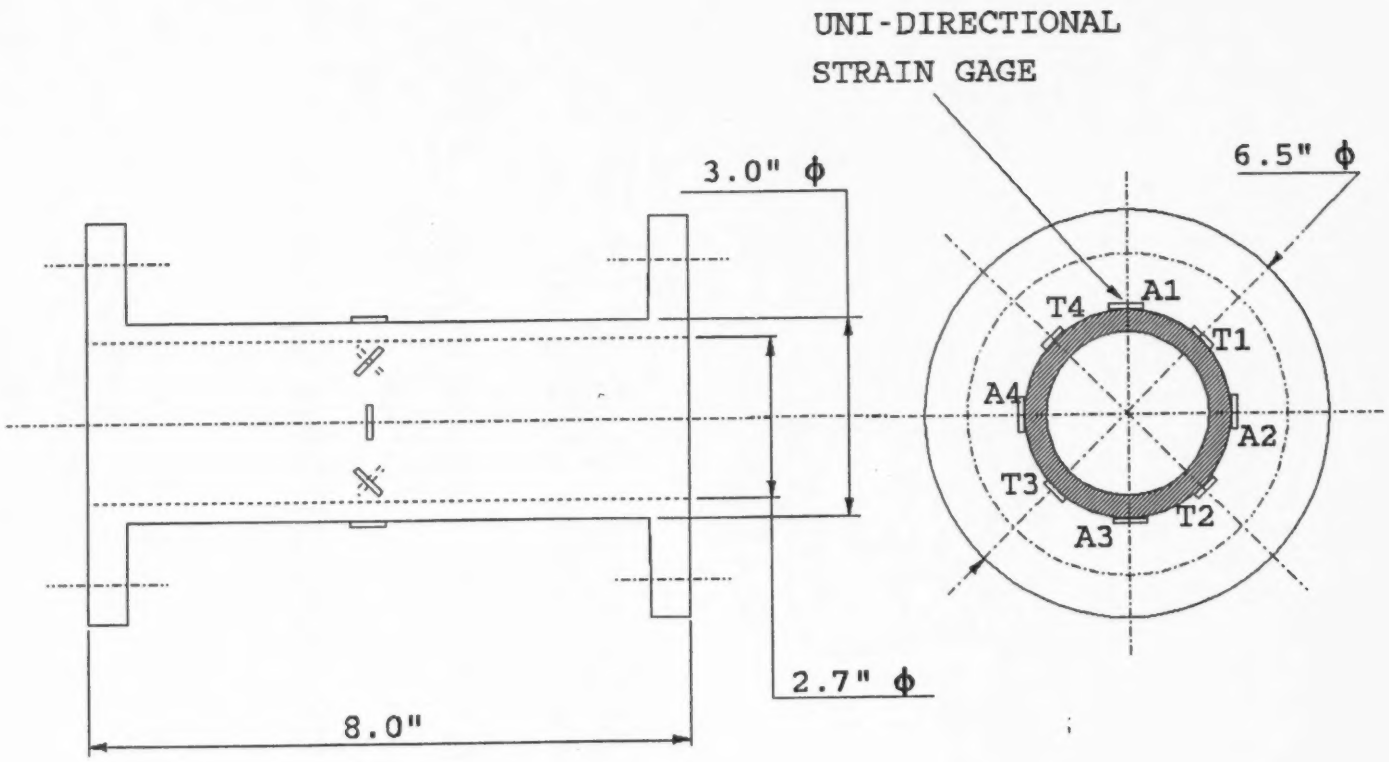

A1,A2,A3,A4 - STRAIN GAGES FOR AXIAL LOAD MEASUREMENT

T1,T2,T3,T4 - STRAIN GAGES FOR TORQUE MEASUREMENT

Figure 5.1
Arrangement of strain gages on the load cell

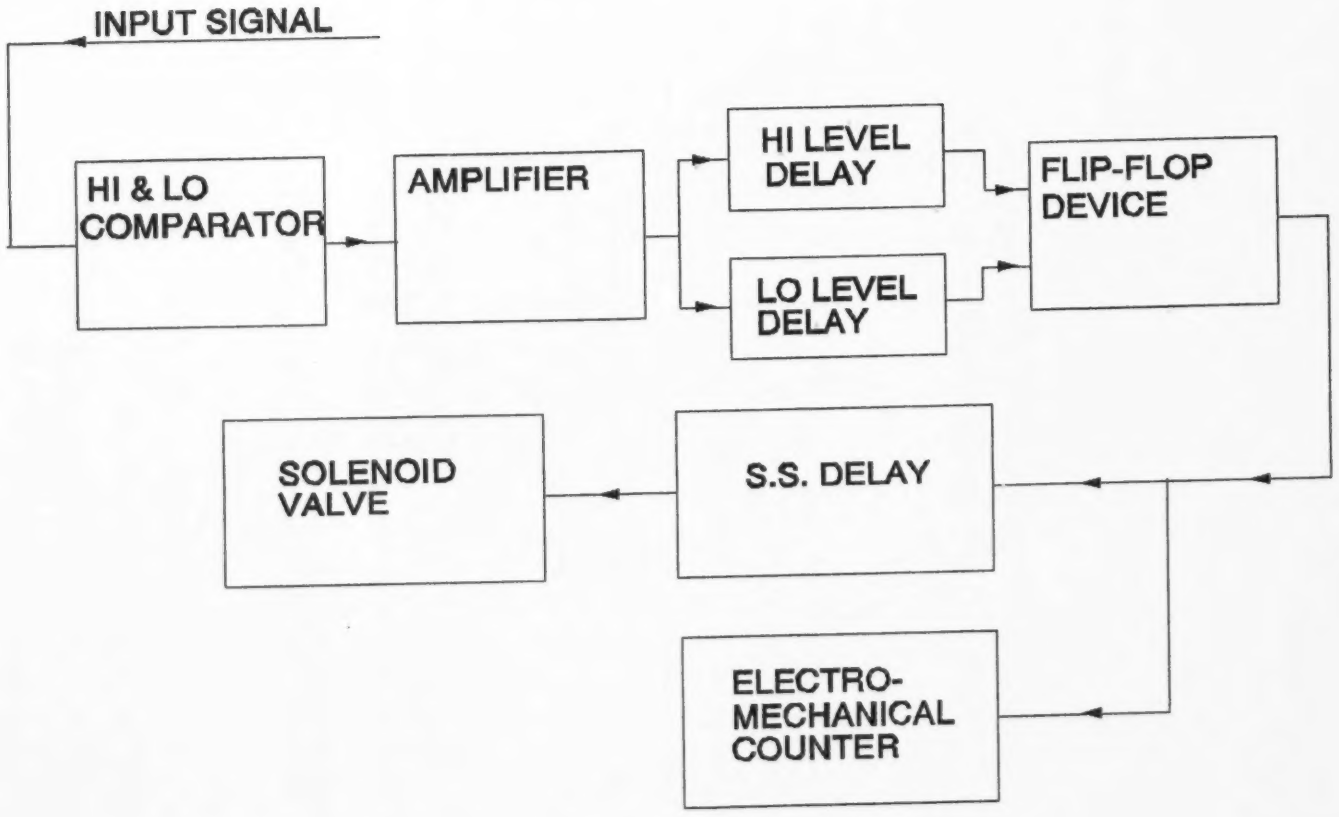

Figure 5.2
Block diagram of the automatic control circuit for cyclic pressure test

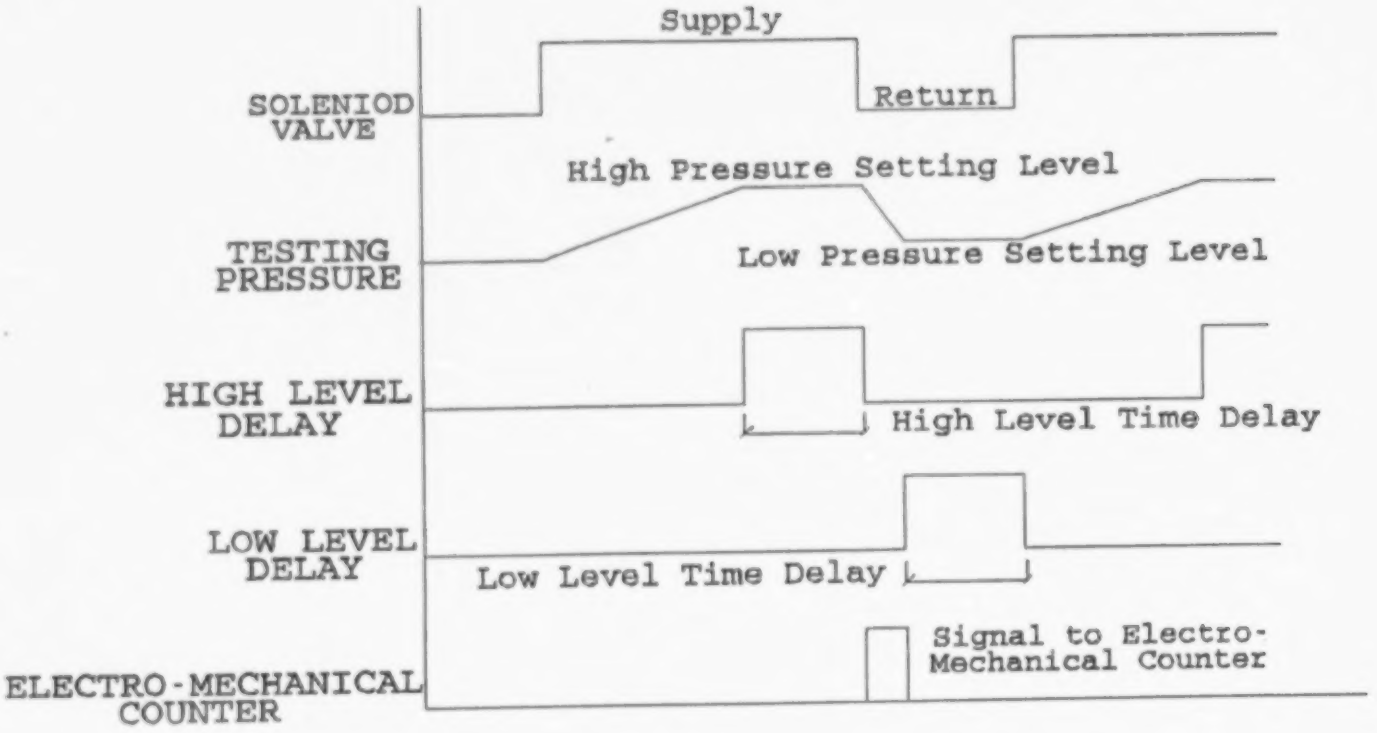

Figure 5.3
Timing diagram for the automatic control logic

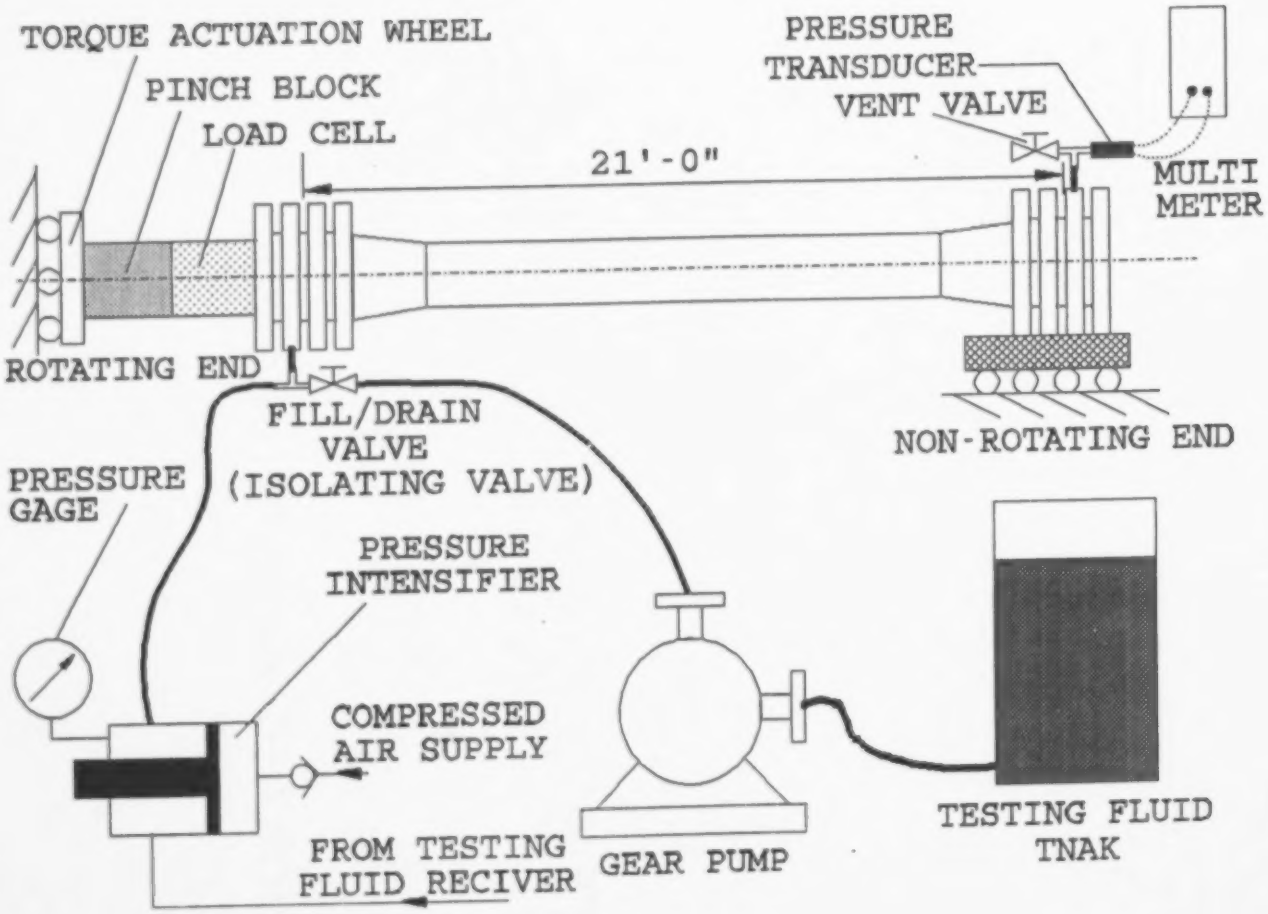

Figure 5.4
Arrangement of the test apparatus in testing of pipe "C"

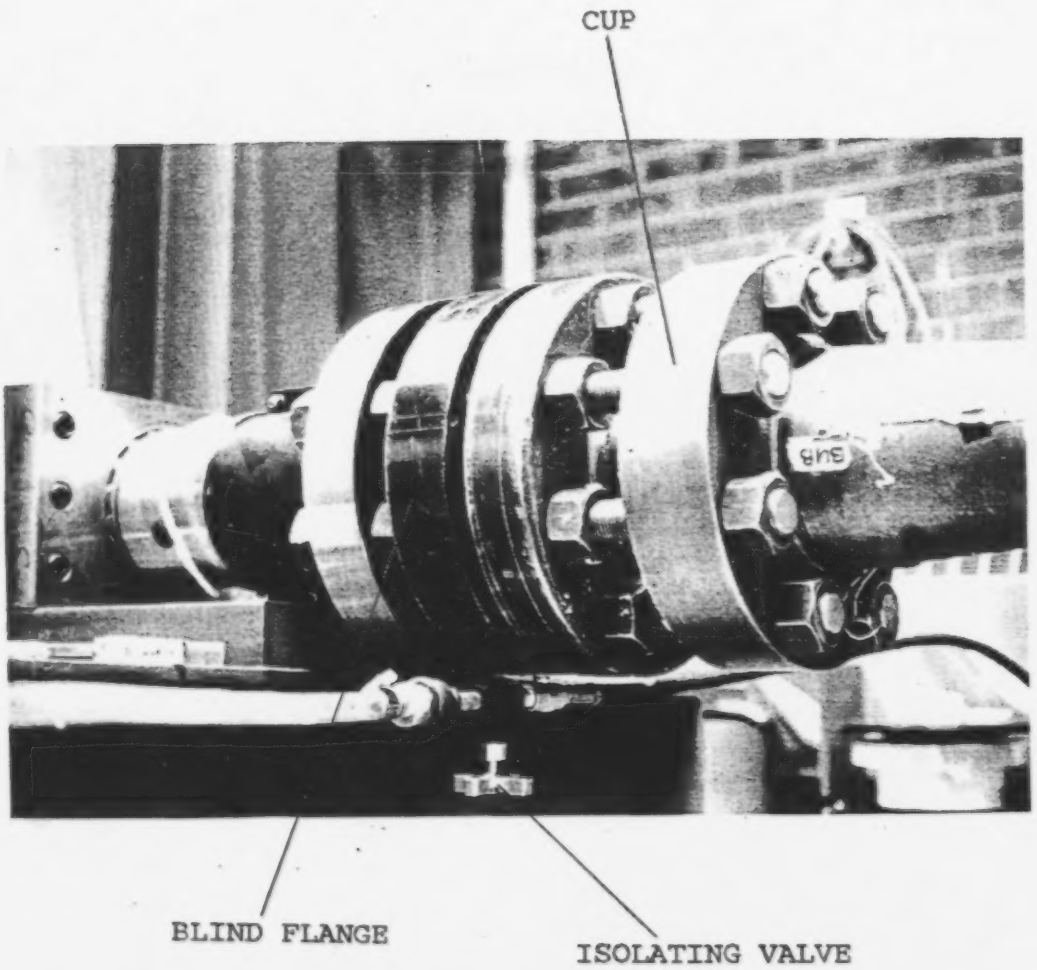

Figure 5.5
Rotating end with the isolating valve

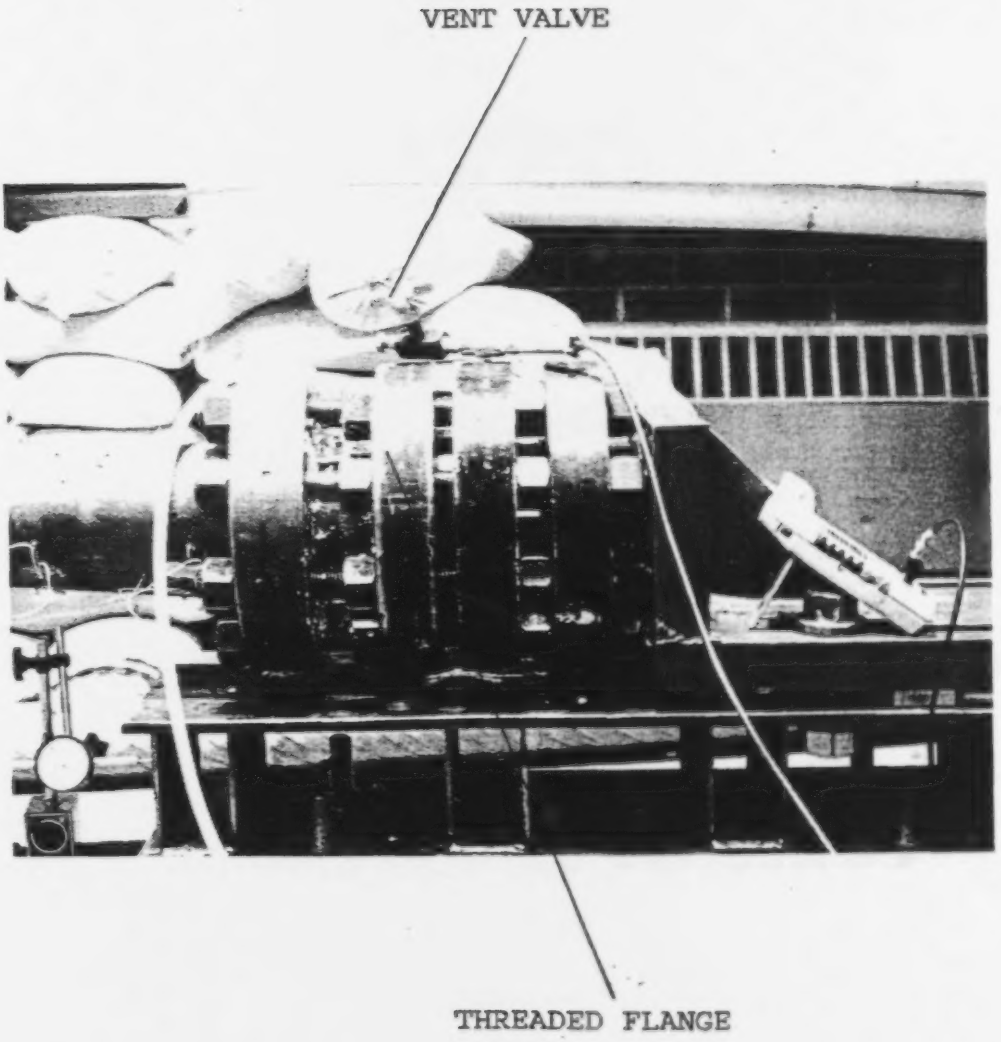

Figure 5.6
Non-Rotating end with the vent valve

Chapter 6 Results and Discussion

Pipe "C" burst at 3,000 psi during the static pressure test. The measurements as well as observations during the test, and the test results are described in this chapter. After failure, the pipe specimen was dissected carefully and inspected visually. The reasons for the failure of the pipe are discussed in this chapter. For the sake of discussion, the pipe is divided into three areas, the end connection domain , the transition area and the pipe domain. Figure 6.1 shows the definition of each area in the pipe.

6.1 Data and observations

Data

Table 6.1 lists all the measurement data collected during the static pressure test of pipe "C".

Table 6.1
Measurements taken in testing of pipe "C"

Step	Pressure	Rotation	Axial Movement	Transverse Movement	Diameter
0	52.5 psi	0°	0"	0"	3.85"
1	1000 psi	12.6°	0"	1/32"	3.86"
2	1017 psi	14°	0"	0"	3.86"
3	27 psi	1.1°	0"	-1/32"	3.85"
4	35 psi	0°	0"	0"	3.85"
5	2010 psi	24.8°	0"	1/16"	3.875"
6	2030 psi	28.1°	0"	1/16"	3.87"
7	25 psi	4.3°	0"	1/32"	3.855"
8	42 psi	0.54°	0"	1/64"	3.865"
9	3024 psi	36.7°	1/32"	1/8"	No data

Observations during the test

1. The pipe appeared to be straight before the test.
2. When the pipe was first loaded to 1,000 psi, noise was generated from the composite strips. It is believed that the noise was due to separation between the glass fibre and the polyester matrix.
3. The pipe rotated in the direction of the outer hoop layer during pressurization. It recovered to its original position after each pressurization and de-pressurization cycle.
4. The noise level was higher at 2,000 psi, and higher again at 3,000 psi.
5. Prior to burst, the transition area of the pipe was observed to expand significantly at the non-rotating end.
6. Bulging of the pipe at the rotating end was also observed.
7. Polyurethane outside the cup at the non-rotating end was broken at 3,000 psi before the pipe failed.
8. Cracking of the polyurethane outside the cup was observed at the rotating end.
9. The pipe failed explosively within the first six inches of the pipe outside the cup of the non-rotating end.
10. The pipe held 3,000 psi for three minutes.
11. The pipe rotated back to its original position after failure.

Observations after the pipe was dissected

Figure 6.2 shows the failure position of each layer. The non-rotating end of the pipe was dissected. The observations of each layer are listed below.

1. Liner

   Two and a half inches of tearing was observed along a line parallel to the inner helix.

2. Inner hoop layer

   Both strips failed on a line parallel to the inner helix strips immediately above the tearing of the liner. The failure configuration of the strips is shown in figure 6.3.

3. Inner helix layer

   One strip was broken along a line coinciding with respect to the failure position of the inner hoop strips. The failure configuration of the strip is shown in figure 6.4.

4. Outer helix layer

   No visible damage was observed.

5. Outer hoop layer

   Two adjacent strips failed at a position near to the tearing of the liner.

6. General observation

   The helix angle of all the structural layers except the inner hoop layer decreased in the transition area as a result of assembling the end connection. The damaged structural layers and the liner are all at one side of the pipe in the transition area.

6.2 Calculation results and discussion

Calculation results

Table 6.2 lists the theoretical calculations of the prototype under 3,000 psi internal pressure. The equations in section 2.2 were used in the calculations. The tensile modulus of the composite strips is taken as 3.5×10^6 psi. Nominal radius, which is one and a half inches, was used in the calculations. Both design parameters and manufacturing parameters are used in the calculation.

Table 6.2
Calculations for pipe "C" under restrained capped ends condition at 3,000 psi internal pressure

p_c (psi)	σ_o (ksi)	σ_e (ksi)	T_{net} (ft-lb)	ϵ_z (%)	ϵ_θ (%)	CAL. PARA.
207.4	68.05	21.09	0	-0.06	2.58	DESIGN
194.8	60.55	17.95	0	-0.03	2.27	MANUF.

Discussion

The helix angles are such that the inner and outer helix layers, and outer hoop layer were observed more axially aligned (smaller helix angle) in the transition area than that in the pipe domain. The helix and the outer hoop layers were disturbed in the transition area during assembly of the end connection. The helix strips were not wrapped flat on the cylindrical surface of the cone, giving more slack in these structural layers in the transition area than in the pipe domain. In addition, any uneven slack in these disturbed layers would explain the uneven bulging of the pipe in the transition area.

The pipe exhibited zero strain when it was pressurized, a result as expected in the original design calculation. However, the pipe rotated in the direction of the outer hoop layer during pressurization. The imbalance between the relatively loose outer hoop layer with respect to inner hoop layer in the transition area could have caused a rotation of the pipe in the direction observed. It is believed that the structural layers re-orientated

themselves to find a new equilibrium position. Whereas the stress in the outer hoop layer increased during pipe rotation, the stress in the inner hoop layer decreased. This was due to rotation of the pipe in the direction of the outer hoop layer which caused the outer hoop layer to tighten against the layers beneath. As a result, the contact pressure beneath the outer hoop layer would increase during pipe rotation. In the pipe domain, the tightening effect of the outer hoop layer against the structural layers beneath would increase the contact pressure between structural layers. This result suggests that the structural layers in the pipe domain did not exhibit solid radial contact until the observed rotation occurred.

The pressure drop across the inner layer may be greater than that across the outer layer than what had been modelled. Hence, the inside structural layers would carry higher stress. This could contribute to the pipe rotation at equilibrium. The polyurethane outside the cup at the non-rotating end was broken prior to the pipe failure. The fracture of the polyurethane outside the cup must be due to the radial expansion of the pipe in the transition area. The burst of the polyurethane could cause some damage to the outer hoop layer. This damage combined with the tensile stress in the outer hoop layer could have caused the outer hoop layer to fail first.

After failure of the outer hoop strips, the inner hoop strips would have to carry higher radial load. This higher stress in the inner hoop strips would cause them to fail. Figure 6.3 shows the failure configuration of the inner hoop strips. In reference to [10], the tensile failure of the hoop strips may be enhanced by weak bonding strength between the fibre and the resin. Therefore, a composite material strength is unknown, it might not be as high as was expected. However, it is believed that the uncertainty of the composite material strength was not the primary reason for the failure.

The inner helix strip failed just above the failed inner hoop strips. Figure 6.4 shows the configuration of the failed inner helix strip. A clear cut was observed perpendicular to the direction of fibre. This kind of failure was not normally found in the structural strips. It is believed that this helix strip was not only broken by tensile stress, but it was also destroyed by the burst of the liner and the explosion of other strips.

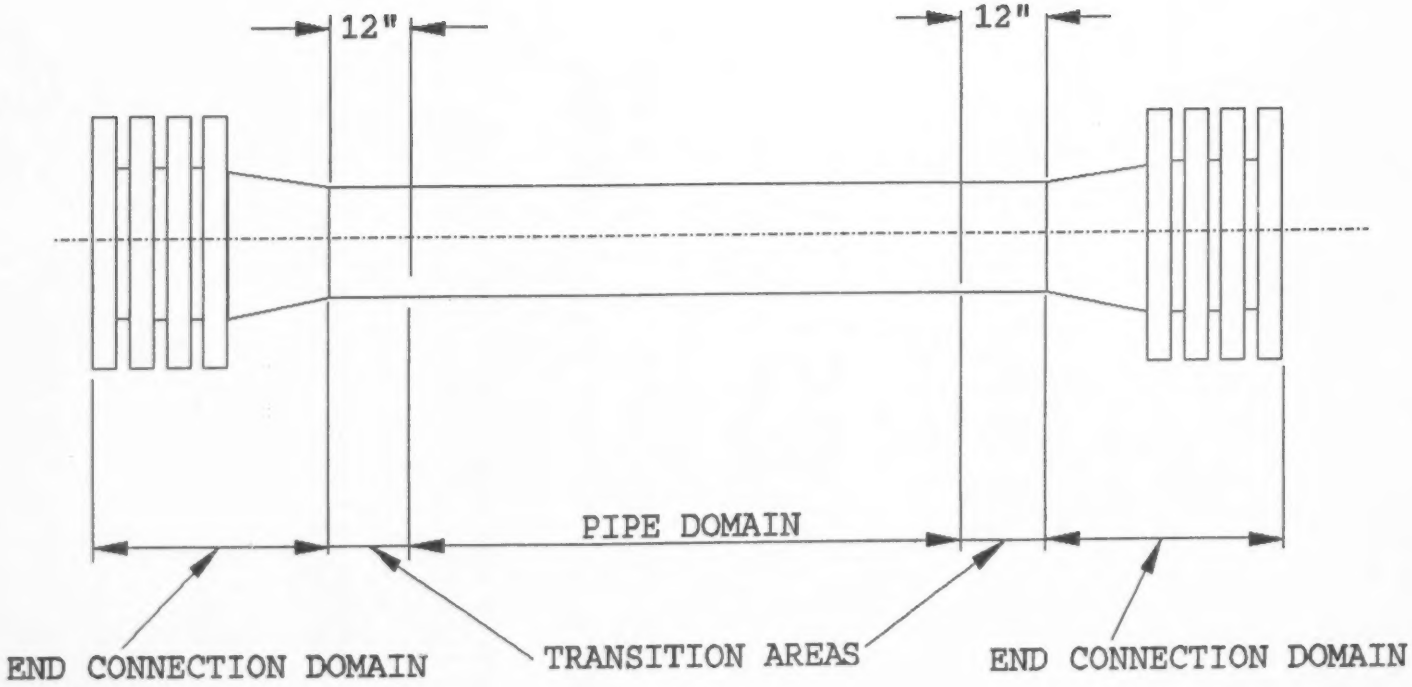

Figure 6.1
The measurements of end connection domain, transition area and pipe domain

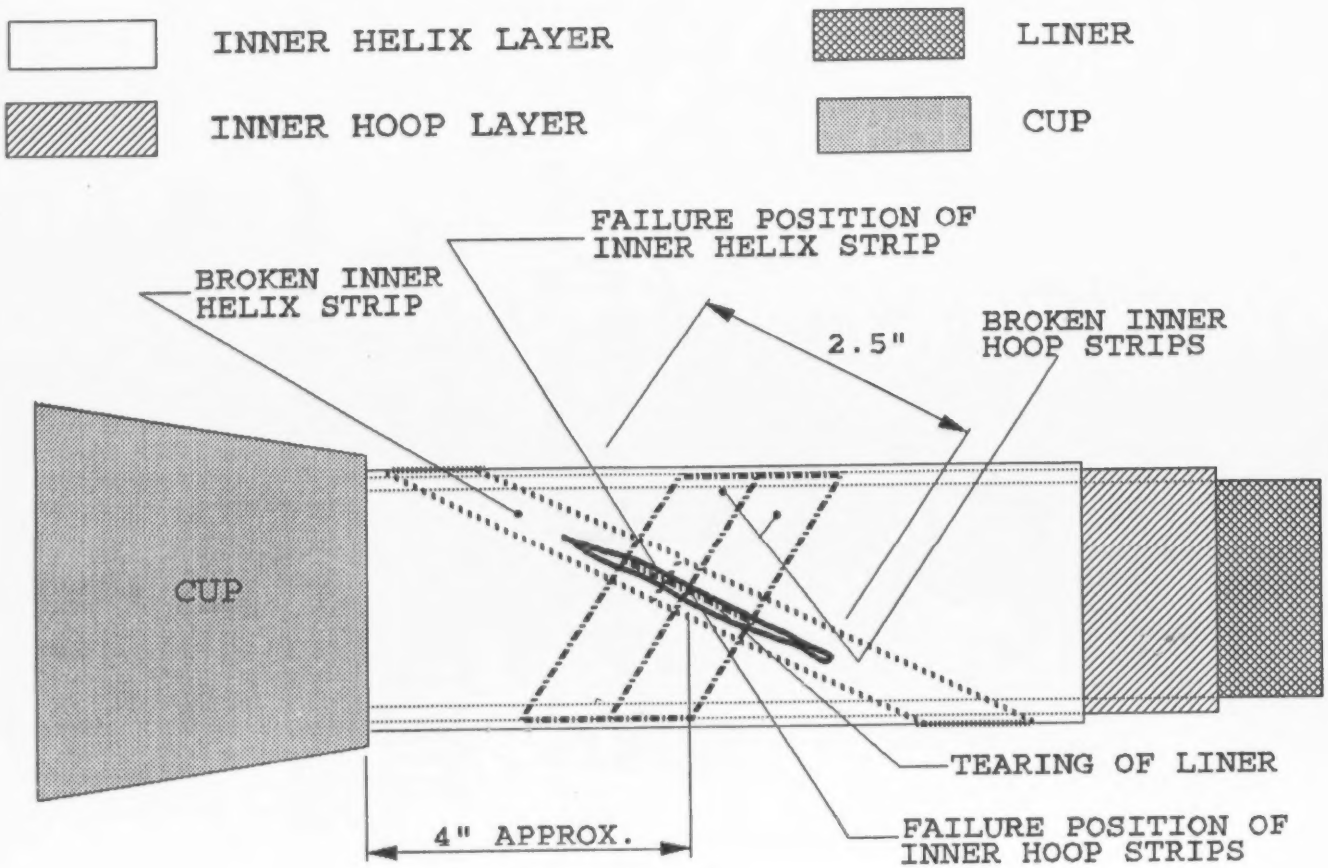

Figure 6.2
Relative position of the failed layers

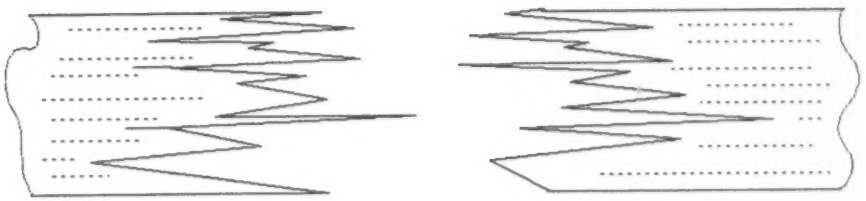

Figure 6.3
Failure configuration of the hoop strips

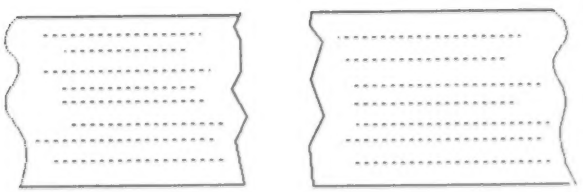

Figure 6.4
Failure configuration of the helix strip

Chapter 7 Pipe Modification

After the completion of the static pressure test of pipe "C" mentioned in Chapter 6, an analysis of the results of the test generated much useful information. A prototype called pipe "D3" was designed and manufactured based on the information obtained from the testing results of pipe "C". Pipe "D3" was designed to have a maximum burst pressure of 11,000 psi. An unrestrained static pressure test was conducted on pipe "D3". This chapter discusses the changes in the pipe design, end connection modifications, testing procedure and the results obtained from the proof test of pipe "D3".

7.1 Pipe design and end connection modification

Pipe design modification

A nominal radius was used in all equations for the design calculation of pipe "C". It was observed in the proof test of pipe "C" that the specimen rotated in the direction of the outer hoop layer during pressurization, which showed in an unbalance in the design of the pipe. Pipe "D3" was modified in three ways. It was designed for a higher pressure than pipe "C" with a burst pressure of 11,000 psi. Based on observation of pipe "C" under pressure, it was observed that the contact pressure was lower than the model predicted. Based on this, the model was corrected to increase the thickness of the hoop structure. The outer hoop layer was moved from being the outermost layer to being adjacent the inner hoop layer. As mentioned in section 6.3, it was believed that the pressure drop across the inner layers of the structure is higher than across the outer layers. This modification helped to obtain a better load distribution between the hoop layers. It was expected this would provide a torque balancing effect.

Table 7.1 shows the physical dimensions of pipe "D3". Equations from section 2.2 were used to calculate the stress and torque generated in each structural layer. It was found that pipe "D3" should show zero net torque, and that the axial strain would be one point six three percent at 11,000 psi internal pressure based on the design parameters of the pipe.

Table 7.1
Designed parameters of pipe "D3"

LAYER	I.D.	THICKNESS	O.D.	α	ϕ	NO. OF STRIPS	HAND
Liner	2.892"	0.204"	3.3"				
Inner Hoop	3.3"	0.120"	3.54"	70.0%	78.08°	2	Left
Outer Hoop	3.54"	0.120"	3.78"	75.0%	80.25°	4	Right
Inner Helix	3.78"	0.120"	4.02"	75.0%	28.00°	10	Left
Outer Helix	4.02"	0.120"	4.26"	75.0%	32.5°	10	Right

End connection modification

The slack in the outer hoop layer of pipe "C" at the transition area could be eliminated by moving the outer hoop layer from the outermost location to the position adjacent to the inner hoop layer. Due to the large helix angle of the outer hoop strips, they were very difficult to wrap tightly on the cone surface of the cone in the end connection assembly of pipe "C". After the outer hoop layer was moved adjacent to the inner hoop layer, both of these hoop layers were inserted inside the cone of the end connection assembly. Therefore, both hoop layers were not disturbed during assembly of the end connection.

Secondly, the number of strips in the inner and outer helix layers were equal in pipe "D3", this also provided for a more convenient means of braiding of the strips over the last six inches of the cone. This also helped to spread out the helix strips more evenly on the cone. Therefore, a better load distribution on the braided injected structure could be achieved when the pipe was loaded.

Thirdly, the radial clearance between the outside diameter of the outer hoop layer and the internal surface of the cone was sixty thousandth of an inch in pipe "C". The radial clearance was reduced to forty thousandth of an inch in pipe "D3". This gave a

better alignment between the pipe domain and the end connection domain.

Fourthly, a better alignment of the helix strips on the cone surface could be improved by using a longer cup (see figure 7.1). The length of the cup should be long enough to cover beyond the take off point of the helix strips. The longer cup was achieved by attaching a nose to the pipe end of the cup. This nose effectively replaced the position of the injected polyurethane outside the cup. The injected polyurethane inside the nose could remove the slack of the disturbed helix strips. Since the longer cup covered the take off point of the helix strips, there would be less bending and twisting in the helix strips when the pipe was loaded.

Finally, the helix angle of the helix strips wrapped on the cone surface had been defined and this helix angle was followed during the end connection assembly. With this helix angle, the helix strips were wrapped tightly on the cone surface.

Figure 7.1 shows the modified end connection used in pipe "D3".

7.2 Testing procedure and test results

Testing procedures

The arrangement of test apparatus in static pressure test of pipe "D3" was the same as in the hydrostatic test of pipe "C". The hydrostatic test of pipe "D3" was performed with capped unrestrained ends on the pipe. The pipe was tested to 5,000 psi internal pressure. The procedure of the test was as follows:

1. The pipe was pressurized for
   - three cycles of zero to 1,000 psi.
   - three cycles of zero to 2,000 psi.
   - three cycles of zero to 3,000 psi.
2. The pipe was pressurized for two cycles of zero to 4,000 psi.
3. The pipe was pressurized from zero to 5,000 psi and held for ten minutes.
4. The pressure inside the pipe was brought back to zero psi.

Test results

The pipe was tested up to 5,000 psi. The testing pressure was measured by the calibrated pressure transducer used in the proof test of pipe "C". The axial movement was measured by using a dial gage, which was held on the floor during the test. A pointer was attached to the rotating shaft of the testing facility for pipe rotation measurement, and indexed with a protractor. No transverse movement was measured at the non-rotating end during the test. There was no measurement taken of the pipe diameter during the test. Table 7.2 summarizes the measurements taken during the test.

Equation 2.22 was used to calculate the theoretical axial strain of the pipe under internal pressure. It was found that the theoretical values were about thirty percent lower than the measured values. In addition, pipe "D3" was designed for zero rotation during pressurization, it was found that the rotation increased with increasing test pressure. The rotation was in the direction of the outer helix layer. There was no apparent bulging observed during the test.

The test results of pipe "D3" were superior to that of pipe "C". It was evident from the modifications mentioned in sections 7.2 and 7.3 that the pipe design and end

connection modifications were responsible for the improvement.

Table 7.2
Measurements taken in testing of pipe "D3"

Ave. Pressure (psi)	Ave. Rotation	Ave. Axial Growth (in.)	Theoretical Axial Strain ε_z (%)	Ave. Axial Strain (%)
1011	0.3°	0.327	0.0924	0.17
2019	2.7°	0.462	0.184	0.24
3032	4.63°	0.707	0.276	0.368
4024	8.5°	No data	0.366	No data
5015	No data	1.199	0.456	0.623

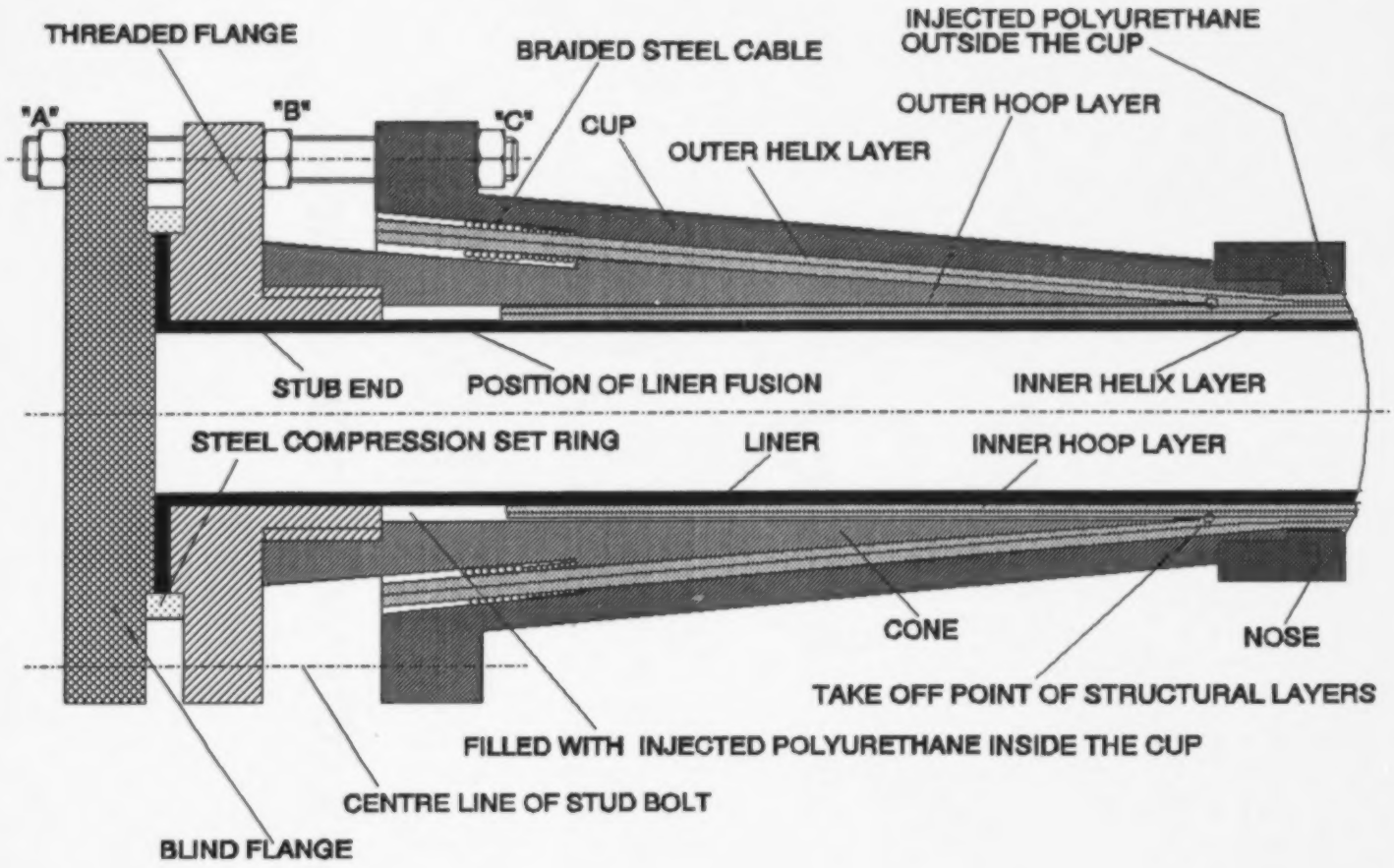

Figure 7.1
End connection assembly of pipe "D3"

Chapter 8 Conclusion and Recommendations

8.1 Conclusion

One objective of this study was to develop some equations governing the behaviour of this flexible composite tubular structure under different loading conditions.

The equations for both unrestrained and restrained end pipes not including the structural contribution of the liner had been developed prior to this study. The equations including the liner as a structural component were developed in this study. In addition, thermal effect on an unrestrained end and a restrained end pipe was investigated for the simple model and the complex model. This included a determination of the contact pressure due to thermal deformation. It was shown that the previous equations developed were a special case of those developed in this thesis. The thermal stress developed in a prototype was calculated.

The second objective was the design of an end connection for pressure testing. The end connection provides a standard connecting flange at the pipe end in order to connect the pipe to conventional equipment. This objective was achieved.

The third objective was to carry a pressure test to prove the pressure capacity of pipe "C". Pipe "C" was designed for zero strain and zero torque under internal pressure. Although zero strain on the pipe was observed in the test, target testing pressure of 5,000 psi was not achieved in the proof test of pipe "C". Pipe "C" burst explosively at 3,000 psi internal pressure. Although the test was not successful, much useful information was obtained for the future pipe development. Pipe design and end connection design were modified and another prototype "D3" was manufactured. Unrestrained test was conducted on pipe "D3", the target testing pressure of 5,000 psi was achieved.

Some special equipment was designed and manufactured to facilitate the planned pipe tests. The major equipment required for these tests were developed, although some equipment was not used in the proof tests of pipe "C" and pipe "D3". This equipment can be used in further development and testing of the pipe.

8.2 Recommendations

1. Pipe "D3" was designed for zero rotation, however the pipe rotated during the test. Therefore, the equations used in pipe design need to be modified in order to better predict the pipe behaviour. It is suggested that the pressure drop across each structural layer needs to be further refined in order to have better modelling equations.
2. The equations developed in this study are only applicable to a straight pipe. However, a curved pipe may occur in a practical application, since this continuous pipe can follow any curve or slope during installation.
3. The buckling behaviour of the pipe under axial compression should be considered. Movements of connecting equipment can cause compressive load on an installed pipe. Under such conditions, problems in buckling of the liner and composite structure should be studied.
4. It is also necessary to carry out stress analysis on buckling of the pipe resulting from external pressure. The maximum external pressure causing the pipe to collapse should be determined, since offshore flexible risers is one of the major applications for this flexible pipe.
5. Pipe rotation was observed during the pipe tests, the reason for pipe rotation is unknown. This pipe rotation phenomenon requires modelling.

The results obtained from experiments are important for further development of the pipe. Experiments should be performed in each of the areas for which the theory has been developed. A lower modulus liner should be used for prototype testing because the liner would not have structural contribution in a practical application. Moreover, because the HDPE liner might not exhibit creep completely during the tests, the equations should be extended to include the viscoelastic behaviour of the liner.

Filament winding was the manufacturing method used to make the prototypes. Although it is a rather simple manufacturing process, a lot of air bubbles were trapped in the polyester resin. These air bubbles could weaken the structural strips. In addition, the variation of the tensile strength of the structural strips is significant. Some errors in the results of calculations could occur because the manufactured dimensions of the pipe

are different from the designed dimensions. Experimental results suggest that there is a small space between structural layers, this space is called construction allowance. This construction allowance needs further investigation. In addition, a better quality control system in pipe manufacturing should be used to improve the prototype quality.

Bibliography

1. J. Neffgen, *Integrity Monitoring for Flexible Pipes*, Pipes & Pipelines International, May - June 1988, pp 7 - pp 14.

2. Dr. D.R. Budney, *Engineering Report*, Composite Technologies Inc., 1992. (Confidential)

3., J.J. Feret, C.L. Bournazel, *Calculation of Stresses and Slip in Structural Layers of Unbonded Flexible Pipes*, Journal of Offshore Mechanics and Arctic Engineering, Transactions of ASME, August 1987, volume 109, pp 263 - pp 269.

4. J.G. de Oliveira, Y. Goto and T. Okamoto, *Theoretical and Methodological Approaches to Flexible Pipe Design and Application*, Offshore Technolory Conference, May 6 - 9 1985, pp 517 - pp 526.

5. Y. Goto, T. Okamoto, M. Araki and T. Fuku, *Analytical Study of the Mechanical Strength of Flexible Pipes*, Journal of Offshore Mechanics and Arctic Engineering, Transactions of the ASME, August 1987, volume 109, pp 249 - pp 253.

6. Veritec Offshore Technology and Services A/S, *Guidelines for Flexible Pipes*, 1987, pp 38 - pp 39.

7. R. Freiheit, *Tensile Testing Report*, Composite Technologies Inc., 1992. (Confidential)

8. American Society for Testing and Materials, *ASTM D2992 - 87, Practice for Obtaining Hydrostatic or Pressure Design Basis for "Fibreglass" (Glass-Fibre-Reinforced Thermosetting-Resin) Pipe and Fitting*, Annex A2.

9. American Society for Testing and Materials, *ASTM E1003 - 84, Standard Method for Hydrostatic Leak Testing*, pp 413 - pp 415.

10. R. McCullough, *Concepts of Fibre - Resin Composites*, Marcel Dekker Inc., pp 35 - pp 59.